© 2016. Published by The Company of Biologists Ltd | Journal of Cell Science (2016) 129, 3620-3634 doi:10.1242/jcs.186817

RESEARCH ARTICLE

ARHGEF10 directs the localization of Rab8 to Rab6-positive executive vesicles

Satoshi Shibata[1,¶], Tsubasa Kawanai[1], Takayuki Hara[1,*], Asuka Yamamoto[1], Taro Chaya[1,‡], Yasunori Tokuhara[1,§], Chinami Tsuji[1], Manabu Sakai[1], Taro Tachibana[2] and Shinobu Inagaki[1,¶]

ABSTRACT

The function of ARHGEF10, a known guanine nucleotide exchange factor (GEF) for RhoA with proposed roles in various diseases, is poorly understood. To understand the precise function of this protein, we raised a monoclonal antibody against ARHGEF10 and determined its localization in HeLa cells. ARHGEF10 was found to localize to vesicles containing Rab6 (of which there are three isoforms, Rab6a, Rab6b and Rab6c), Rab8 (of which there are two isoforms, Rab8a and Rab8b), and/or the secretion marker neuropeptide Y (NPY)–Venus in a Rab6-dependent manner. These vesicles were known to originate from the Golgi and contain secreted or membrane proteins. Ectopic expression of an N-terminal-truncated ARHGEF10 mutant led to the generation of large vesicle-like structures containing both Rab6 and Rab8. Additionally, small interfering (si)RNA-mediated knockdown of ARHGEF10 impaired the localization of Rab8 to these exocytotic vesicles. Furthermore, the invasiveness of MDA-MB231 cells was markedly decreased by knockdown of ARHGEF10, as well as of Rab8. From these results, we propose that ARHGEF10 acts in exocytosis and tumor invasion in a Rab8-dependent manner.

KEY WORDS: ARHGEF10, RhoGEF, Membrane trafficking, RabGTPase

INTRODUCTION

Exocytotic vesicles containing newly synthesized secreted or membrane proteins are transported from the Golgi apparatus along a microtubule or actin fiber to the plasma membrane. This process is very important for maintenance of the homeostatic environment and appropriate movement of the cell (Anitei and Hoflack, 2012). A previous proposal suggests that, in migrating epithelial cells, exocytotic vesicles containing matrix metalloproteases are transported near to focal adhesions to sever cell–matrix connections and thus facilitate focal adhesion turnover (Stehbens et al., 2014). Insulin stimulation induces the translocation of GLUT4-storage vesicles to the plasma membrane to promote the uptake of glucose by adipocytes and muscle cells (Dugani and Klip, 2005; Ishikura and Klip, 2008; Chen et al., 2012; Sun et al., 2014). In addition to this pathway, various membrane trafficking pathways involving inter-organelle or retrograde transport or recycling play important roles in the precise coordination of cell functions.

RabGTPases, which belong to the Ras-like small GTPase superfamily, are well-known regulators of these membrane trafficking pathways (Hutagalung and Novick, 2011; Anitei and Hoflack, 2012). Each vesicle that originates from the plasma membrane or various organelles must be transported along the cytoskeleton and tethered to and fused with the target membrane. The Rab family comprises more than 60 members, and specific Rabs must localize to appropriate membranes to ensure the specificity and directionality of trafficking events. For example, Rab5 resides on the early endosome and functions in the fusion of endocytosed vesicles to the endosomal membrane (Hutagalung and Novick, 2011), and Rab7 localizes to the late endosome, where it mediates lysosome biogenesis (Bucci et al., 2000; Maxfield and McGraw, 2004). Rab11a localizes to the recycling endosome to regulate plasma membrane recycling (Ullrich et al., 1996). Recent studies have revealed that exocytotic vesicles expressing Rab6a and Rab8a are transported from the Golgi to the plasma membrane (Grigoriev et al., 2011). In this process, Rab6a is thought to act in both the fission of the exocytotic vesicle from the Golgi and in the transport of the vesicle toward the plasma membrane (Grigoriev et al., 2007; Miserey-Lenkei et al., 2010). Rab8a localizes to exocytotic vesicles in a Rab6-dependent manner, and has been implicated in the docking and fusion of these vesicles to the plasma membrane (Grigoriev et al., 2011). Furthermore, a number of studies have suggested the involvement of Rab8 in various cell functions, including membrane recycling, regulation of cell shape, polarized membrane transport and primary cilia formation (Hattula et al., 2002, 2006; Ang et al., 2003; Nachury et al., 2007; Sato et al., 2007, 2014; Henry and Sheff, 2008). Similar to many other small G-proteins, Rabs function as molecular switches that cycle between GDP- (inactive state) and GTP-bound (active state) forms to control their effectors and thus coordinate specific trafficking pathways. For example, Rabaptin-5, which is required for endosomal fusion, is recruited to the membrane by Rab5 in a GTP-dependent manner (Stenmark et al., 1995; Horiuchi et al., 1997). Through its effector, Rab11 family interacting protein 2, Rab11 interacts with the unconventional myosin protein myosin-Vb to regulate plasma membrane recycling (Hales et al., 2001).

The RhoGTPase family, which comprises 20 members, organizes the actin cytoskeleton to mediate various cellular processes involved in migration, cytokinesis and morphological changes. Among these proteins, RhoA, Cdc42 and Rac1 are well-known inducers of stress fiber and focal adhesion formation, filopodia formation, and lamellipodia formation, respectively, in fibroblasts (Ridley and Hall, 1992; Ridley et al., 1992; Nobes and Hall, 1995). RhoGTPases act as molecular switches, similar to

[1]Group of Neurobiology, Division of Health Sciences, Graduate School of Medicine, Osaka University, Osaka 565-0871, Japan. [2]Department of Bioengineering, Graduate School of Engineering, Osaka City University, Osaka 558-8585, Japan. *Present address: Division of Pathogenesis and Control of Oral Diseases, Graduate School of Dentistry, Osaka University, 565-0871, Japan. ‡Present address: Laboratory for Molecular and Developmental Biology, Institute for Protein Research, Osaka University, Osaka 565-0871, Japan. §Present address: Kagawa Prefectural University of Health Sciences, Takamatsu, Kagawa 761-0123, Japan.

¶Authors for correspondence (sshibata@sahs.med.osaka-u.ac.jp; inagaki@sahs.med.osaka-u.ac.jp)

S.I., 0000-0002-2785-1214

Received 29 January 2016; Accepted 13 August 2016

Journal of Cell Science (2016) 129, 3620-3634 doi:10.1242/jcs.186817

RabGTPases. Rho activity is controlled by guanine nucleotide exchange factors (GEFs), GTPase activating proteins (GAPs), and GDP dissociation inhibitors (GDIs). GEFs catalyze the exchange of GDP for GTP to activate Rho proteins, GAPs enhance the slow intrinsic GTPase activity of Rho proteins, and GDIs prevent the dissociation of GDP from Rho proteins. Rho activity is therefore precisely controlled by each RhoGEF, both spatially and temporally. Recent accumulating evidence has indicated a relationship between Rho-family proteins and the membrane trafficking pathway (Croisé et al., 2014).

ARHGEF10 is a Dbl-type RhoGEF, a class of 69 proteins that contain the Dbl homology (DH) GEF catalytic domain. ARHGEF10 acts as a GEF for RhoA-subfamily members, including RhoA, RhoB and RhoC (Mohl et al., 2006; Chaya et al., 2011). Previously, Verhoeven et al. have indicated that a missense mutation of ARHGEF10, in which threonine is changed to isoleucine at codon 332 (T332I), is associated with slowed nerve conduction velocities and thin peripheral nerve myelination in humans, without any obvious clinical symptoms in the affected individuals (Verhoeven et al., 2003). We have previously revealed that overexpression of the T332I mutant in HeLa and Schwann cells induces cell contraction as a result of constitutively enhanced GEF activity (Chaya et al., 2011). This result led to a proposal that the phenotypes observed in T332I-mutant-expressing peripheral nerves were caused by aberrant GEF activation. However, the fundamental function of ARHGEF10 remains unknown.

To elucidate the function of ARHGEF10, we performed cytochemical and functional analyses using a monoclonal antibody against ARHGEF10, and overexpression and knockdown techniques. We demonstrated that both endogenous and exogenous forms of ARHGEF10 localized to Rab6- and Rab8-positive exocytotic vesicles. Overexpression of an N-terminal-deleted form of ARHGEF10 led to the generation of large vesicle-like structures containing Rab6 and Rab8. Furthermore, knockdown of ARHGEF10 impaired the localization of Rab8 to exocytotic vesicles. Moreover, the invasiveness of MDA-MB231 cells through a Matrigel-coated membrane was reduced by knockdown of ARHGEF10, as well as of Rab8. These results imply that ARHGEF10 functions in Rab8-related membrane trafficking pathways.

RESULTS

The antiARHGEF10 monoclonal antibody specifically recognizes ARHGEF10

A monoclonal antibody, antiARHGEF10, was raised against the N-terminal region of ARHGEF10 to facilitate an analysis of the subcellular localization of this protein. When a total HeLa cell extract was subjected to immunoblotting, antiARHGEF10 specifically recognized a protein slightly smaller than 200 kDa (Fig. 1A). This recognition was lost after knockdown of ARHGEF10 (Fig. 1B). Immunoblotting of an ectopically expressed Myc-tagged ARHGEF10 yielded a band with a similar molecular mass to that previously recognized (see later). AntiARHGEF10 also recognized ARHGEF10 in HEK293T and CHO cells (Fig. S1A). Immunofluorescence analysis using antiARHGEF10 revealed a diffuse distribution and cytoplasmic vesicle-like puncta in HeLa cells (Fig. 1C). AntiARHGEF10 staining formed similar puncta in MDCK and MDA-MB231 cells (data not shown; see later). However, these puncta were lost when ARHGEF10 was depleted by using RNA interference (RNAi) (Fig. 1Dc). When HeLa cells expressing mCherry-tagged ARHGEF10 or mCherry (control) were immunostained with

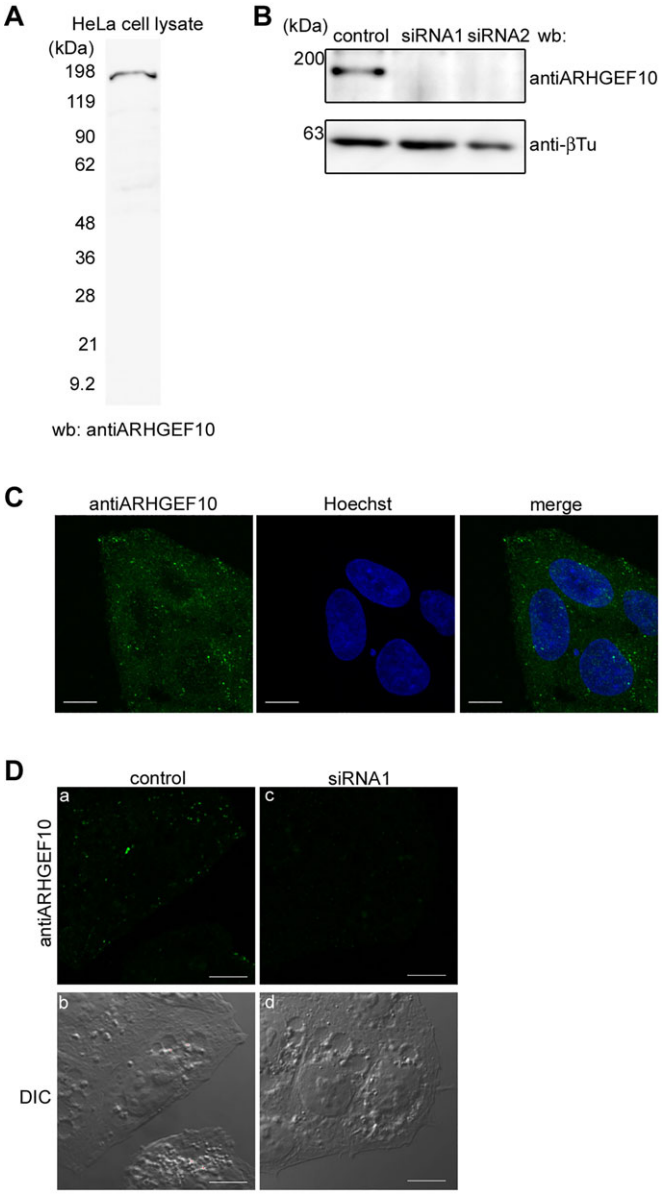

Fig. 1. Generation of an antibody specifically recognizing ARHGEF10. (A) Protein extract from HeLa cell was immunoblotted with the mouse antiARHGEF10 antibody. antiARHGEF10 specifically recognized a protein slightly smaller than 200 kDa. Molecular masses in kDa are indicated to the left. (B) Protein extract from HeLa cells treated with siRNA directed against ARHGEF10 (siRNA1 and siRNA2) (middle and right lane) or control (left lane) were immunoblotted with antiARHGEF10 (upper panel) and anti-β-tubulin antibodies (anti-βTu, lower panel). The bands recognized by antiARHGEF10 were specifically decreased by knockdown of ARHGEF10. Molecular masses in kDa are indicated to the left. (C) HeLa cells were immunostained with antiARHGEF10 (left panel). antiARHGEF10 recognized cytoplasmic puncta. Nuclei were labeled with Hoechst 33258 (middle panel). Merged images are shown in the right-hand panels. *z*-stack confocal images were acquired with a confocal microscope. Scale bars: 10 µm. (D) Immunocytochemistry was performed using HeLa cells treated with control (a and b) or siRNA1 (c and d) siRNAs. A single focal plane was acquired. These signals were not detected in cells treated with siRNA1 (c). Differential interference contrast (DIC) images are shown in lower panels (b and c). Scale bars: 10 µm.

antiARHGEF10, HeLa cells expressing mCherry-tagged ARHGEF10 exhibited brighter antiARHGEF10 labeling than did non-transfected or mCherry (control)-transfected cells (Fig. S1B). These data indicate that antiARHGEF10 specifically recognizes

Journal of Cell Science (2016) 129, 3620-3634 doi:10.1242/jcs.186817

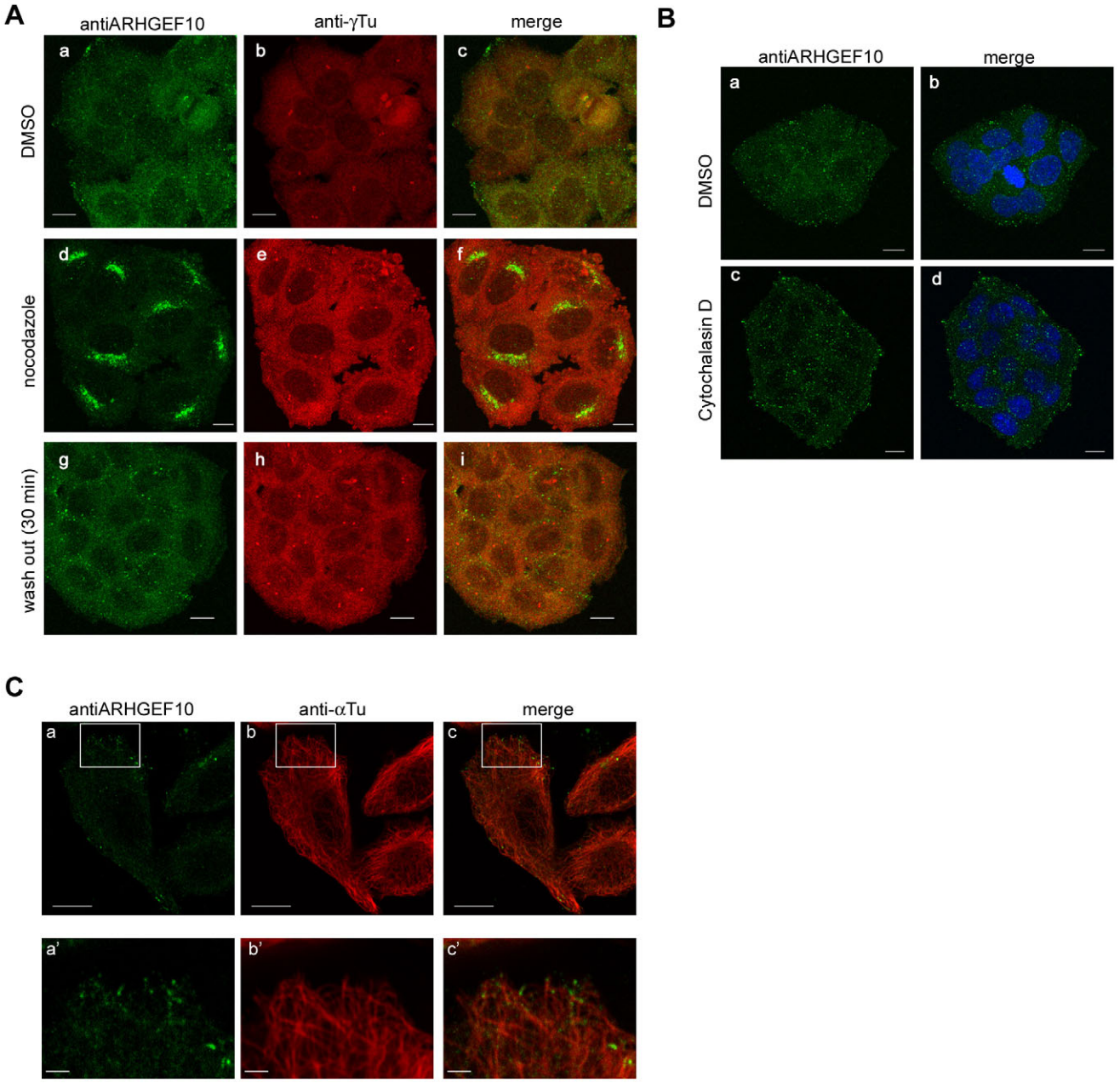

Fig. 2. Localization of ARHGEF10 was altered by depolymerization of microtubules but not of actin filaments. (A) HeLa cells were treated with DMSO (a–c) or 10 µM nocodazole (d–f) for 1 h. These cells were fixed in ice-cold methanol and immunostained with antiARHGEF10 (a and d) and anti-γ-tubulin antibody (anti-γTu, b and e). After washout of nocodazole, HeLa cells were incubated for 30 min in normal media (g and h). Merged images are shown in the right-hand panels (c,f,i). *z*-stack confocal images were acquired on a confocal microscope. Scale bars: 10 µm. (B) HeLa cells were treated with DMSO (a and b) or 0.1 µM cytochalasin D (c and d) for 1 h. These cells were fixed in 10% PFA and immunostained with antiARHGEF10 (a and c) and counterstained with Hoechst 33258. Merged images are shown in the right-hand panels (b and d). *z*-stack confocal images were acquired on a confocal microscope. Scale bars: 10 µm. (C) HeLa cells were double stained with antiARHGEF10 (a) and anti-α-tubulin antibodies (anti-αTu, b). Merged images are shown in the right-hand panels (c). Scale bars: 10 µm. Higher magnification views of the boxed areas are shown in lower panels (a′–c′). Scale bars: 2 µm. A single focal plane was acquired on a confocal microscope.

ARHGEF10 in immunoblotting and immunocytochemistry analyses.

Disruption of microtubules alters the localization of ARHGEF10

Because cytoskeletons regulate the localization of some proteins (Hutagalung and Novick, 2011; Anitei and Hoflack, 2012), the destruction of these structures might affect protein localization. To examine whether the localization of ARHGEF10 is regulated by the cytoskeleton, HeLa cells were treated with nocodazole, a microtubule-disrupting drug, or DMSO as a control. In DMSO-treated cells, ARHGEF10 was distributed in cytoplasmic puncta (Fig. 2A). In contrast, microtubule disruption induced the accumulation of ARHGEF10 near to the centrosome, as indicated by staining of γ-tubulin (Fig. 2Ad–Af). This accumulation dispersed at 30 min after removal of the drug (Fig. 2Ag–Ai). Although these cells had been fixed in methanol to allow immunostaining of γ-tubulin, similar results were observed in cells that had been fixed in

Journal of Cell Science (2016) 129, 3620-3634 doi:10.1242/jcs.186817

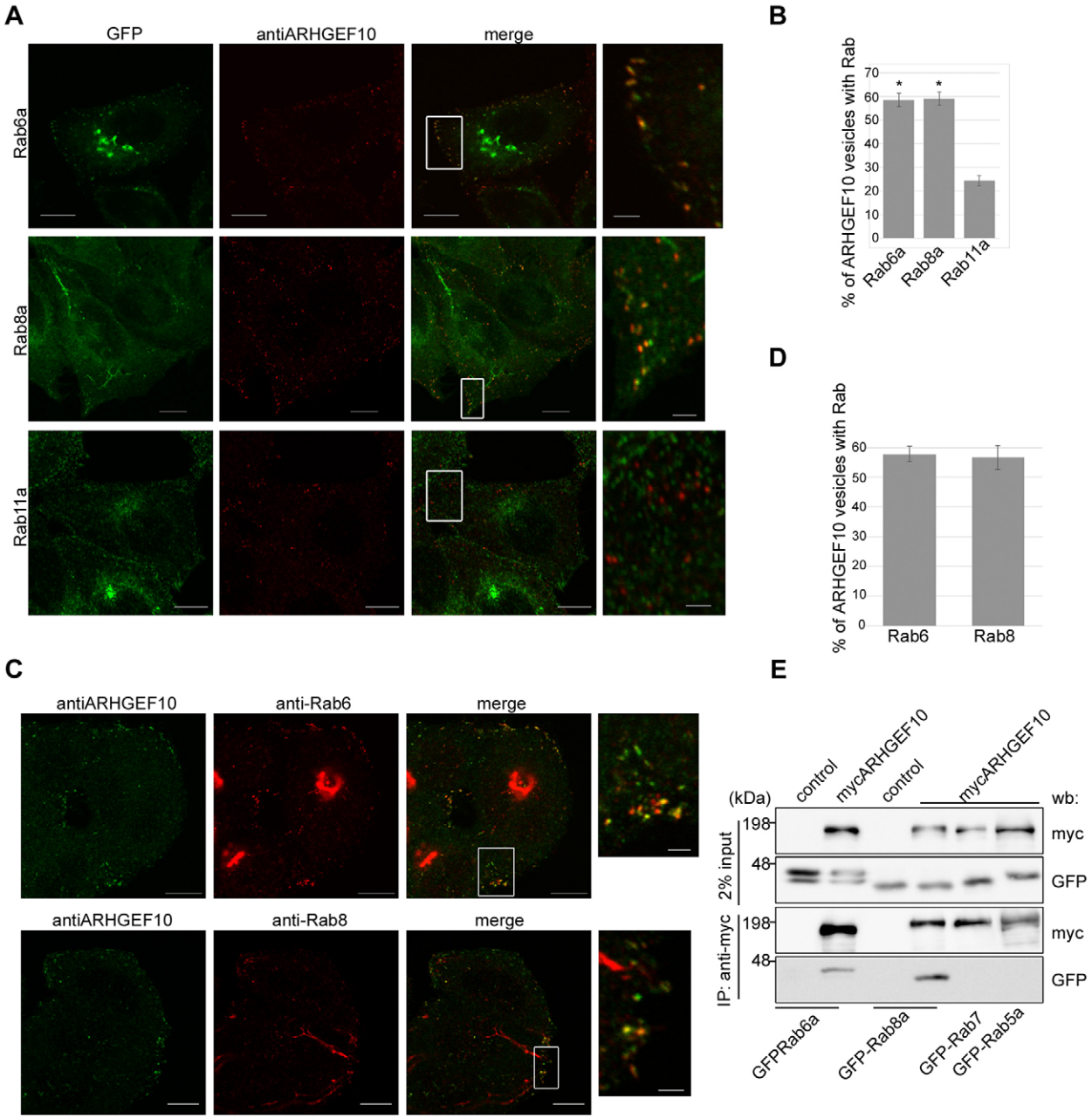

Fig. 3. ARHGEF10 localized to the vesicles containing exogenous or endogenous Rab6a and Rab8a, and interacted with exogenously expressed Rab6a and Rab8a. (A) HeLa cells stably expressing GFP-tagged Rab6a, Rab8a or Rab11a (left panels, green) were stained with antiARHGEF10 (middle panels, red). Scale bars: 10 µm. Higher magnification views of the boxed areas are shown in the right-hand panels. Scale bars: 2 µm. A single focal plane was acquired on a confocal microscope. (B) Colocalization of endogenous ARHGF10 and GFP-tagged Rab6a, Rab8a or Rab11a was quantified using HeLa cells stably expressing each Rab protein. Colocalization efficiency was expressed as a percentage of both ARHGEF10- and GFP-positive vesicles of the total number of antiARHGEF10-positive vesicles. More than ten cells were examined per assay. Error bars indicate s.e.m. (*P<0.01, Student's t-test). (C) HeLa cells were immunostained for endogenous ARHGEF10 (left panels, green) and endogenous Rab6 (upper middle panel, red) or Rab8 (lower middle panel, red). Merged images are shown in the right-hand panels. A single focal plane was acquired on a confocal microscope. Scale bars: 10 µm. Higher magnification views of the boxed areas are shown in the right-hand panels. Scale bars: 2 µm. (D) Percentage of both ARHGEF10- and Rab6- or Rab8-positive vesicles of the total number of ARHGEF10-positive vesicles were calculated. More than 20 cells were examined. Error bars indicate s.e.m. (E) HEK293T cells were co-transfected with pCMV-Myc-control or pCMV-Myc-ARHGEF10 and GFP-tagged Rab (Rab6a, Rab8a, Rab7 or Rab5a) expression plasmids. Total cell lysates (input) were subject to immunoprecipitation (IP) with anti-Myc antibodies. 2% of the total cell lysate and immunoprecipitates were analyzed by western blotting (wb) using anti-myc antibodies and anti-GFP antibodies. Molecular masses in kDa are indicated to the left.

4% paraformaldehyde (PFA) (Fig. S1C). Furthermore, we confirmed that the accumulated antiARHGEF10-immunostaining signals in nocodazole-treated cells were lost upon ARHGEF10 knockdown (Fig. S1C). By contrast, no change in protein localization was observed following treatment with cytochalasin D, which is known to inhibit actin polymerization (Fig. 2B). Furthermore, double staining for ARHGEF10 and α-tubulin, a microtubule component, revealed the partial distribution of ARHGEF10 puncta along the microtubules (Fig. 2C). These results suggest that ARHGEF10 localization is affected by microtubule orientation.

Journal of Cell Science (2016) 129, 3620-3634 doi:10.1242/jcs.186817

ARHGEF10 localizes to Rab6- and/or Rab8-positive vesicles

Immunofluorescence imaging of antiARHGEF10 revealed cytoplasmic puncta that resembled cytoplasmic vesicles, and these findings were affected by microtubule disruption. Many secretory and endocytic vesicles are known to move along microtubules to reach the plasma membrane and target organelles, respectively (Anitei and Hoflack, 2012). These data suggested that ARHGEF10 might localize to such vesicles. To examine this hypothesis, we examined the colocalization of ARHGEF10 with various Rab proteins that are known to exist on cytoplasmic vesicles related to various membrane trafficking processes and that are used as markers of vesicles involved in specific transport pathways. Six GFP-tagged Rab-family proteins were transiently expressed in HeLa cells, and the colocalization of each Rab with endogenous ARHGEF10 was subsequently examined. Among these Rabs, Rab6a and Rab8a were found to colocalize with ARHGEF10 on vesicle-like puncta around the plasma membrane (Fig. S2). To evaluate the colocalization efficiency of ARHGEF10 with each Rab, HeLa cells with stable expression of GFP-tagged Rab6a, Rab8a or Rab11a were immunostained with antiARHGEF10 (Fig. 3A). Although approximately 15% of the ARHGEF10-positive vesicles contained GFP–Rab11, approximately 60% of ARHGEF10-positive vesicles contained GFP–Rab6a or GFP–Rab8a (Fig. 3B). Similar results were obtained in an evaluation of the colocalization efficiency between antiARHGEF10-positive and endogenous Rab8- or Rab6-positive vesicles (Fig. 3C,D). Although Rab6 has been reported to localize to the Golgi, as well as to vesicles (Goud et al., 1990; Grigoriev et al., 2011), ARHGEF10 was not found at the Golgi (Fig. 3C). Furthermore, a previous report has noted Rab8 localization to tubular structures (Hattula et al., 2006). However, we did not observe the alignment of ARHGEF10-positive vesicles along tubular structures, except for a few ARHGEF10-positive vesicles that were observed at or near the edges of these tubules (Fig. 3D). These results indicate that ARHGEF10 localized to Rab6- and/or Rab8-positive vesicles, but not to the Rab6-positive Golgi and Rab8-positive tubular structures, suggesting that ARHGEF10 might interact with both Rab6 and Rab8. To examine whether ARHGEF10 could interact with Rab6 and Rab8, an immunoprecipitation assay using overexpressed Myc-tagged ARHGEF10 and GFP-tagged Rab5a, Rab7, Rab6a or Rab8a (Fig. 3E) was performed. Although no interactions were detected between Myc-tagged ARHGEF10 and GFP-tagged Rab7 and Rab5, Myc-tagged ARHGEF10 was found to interact with GFP-tagged Rab6a and Rab8a. Although similar interactions were observed regardless of Rab6a or Rab8a activity, dominant-negative Rab6a was associated with a slightly reduced interaction, compared with constitutively active Rab6a (constitutively active Rab6a) (Fig. S3A,B). These results indicate that ARHGEF10 localizes with Rab6- or Rab8-positive vesicles and interacts with Rab6 and Rab8.

ARHGEF10 resides on Rab6- and Rab8-positive exocytotic vesicles, and ectopic expression of an N-terminal-truncated ARHGEF10 mutant leads to the generation of large vesicle-like structures containing Rab6 and Rab8

ARHGEF10 was found to localize to Rab6- and/or Rab8-positive vesicles. This suggested that ARHGEF10 might localize to Rab6- and Rab8-double-positive vesicles. To examine this hypothesis, we immunostained HeLa cells that stably expressed GFP-tagged Rab6a with antiARHGEF10 and an anti-Rab8 antibody (Fig. 4A). A total of 50.45%±3.17 (mean ± s.e.m.) of all ARHGEF10-positive vesicles was found to be labeled for both GFP (GFP–Rab6a) and Rab8. These findings strongly suggest that ARHGEF10 localized to Rab6- and Rab8-double-positive vesicles. A recent study indicates that both Rab6 and Rab8 reside on exocytotic vesicles that contain the membrane or secreted proteins and that are transported from the Golgi to the plasma membrane (Grigoriev et al., 2007, 2011). These data prompted us to investigate whether ARHGEF10 localizes to exocytotic vesicles. To examine this possibility, a cell line with stable expression of the secretion marker neuropeptide Y (NPY)–Venus (Nagai et al., 2002) was established, and the localization of ARHGEF10 was compared with that of NPY–Venus. As expected, ARHGEF10 localized to NPY–Venus-positive vesicles (Fig. 4B). An evaluation of the colocalization efficiency between ARHGEF10 and NPY–Venus revealed that 60% of ARGEF10-positive vesicles corresponded with NPY–Venus-positive vesicles (Fig. 4C). A similar colocalization efficiency was also obtained in cells that stably expressed another secretion marker, mCherry fused to Ig κ-chain leader sequence (Ig–mCherry) (data not shown). This secretion marker was also detected in Rab6- and Rab8-positive vesicles and was secreted into cell culture medium (data not shown). Next, to investigate whether ectopically expressed ARHGEF10 could localize to these exocytotic vesicles, the localization of hemagglutinin (HA)-tagged ARHGEF10 in HeLa cells was compared with that of endogenous Rab6 and Rab8. As shown in Fig. 5B,C, although overexpressed full-length ARHGEF10 also localized to Rab6- and/or Rab8-positive vesicles, these punctate signals were slightly ambiguous as a result of increased diffuse distribution of ARHGEF10. Similar to endogenous ARHGEF10, overexpressed ARHGEF10 was not detected on the Rab6-positive Golgi or Rab8-positive tubular structures (Fig. 5B,C). Some overexpressed ARHGEF10-containing vesicles were observed at or near Rab8-positive tubular structures (Fig. 5C). These results indicate that ARHGEF10 localized to the exocytotic vesicles. By contrast, an N-terminal-truncated mutant of ARHGEF10 (lacking residues 1–210 and referred to as 211∼; Fig. 5A) localized not only to Rab6- and/or Rab8-positive vesicles but also to Rab8-positive tubular structures. Furthermore, expression of mutant 211∼ led to the generation of large vesicle-like structures containing Rab6 and/or Rab8. These structures were occasionally found to associate with Rab8-positive tubular structures (Fig. 5Cd′, arrows). These results suggest that the N-terminal region of ARHGEF10 suppresses the mislocalization of ARHGEF10 to Rab8-positive tubular structures, and that ARHGEF10 might also regulate the localization of Rab6 and Rab8.

To confirm the localization of ARHGEF10 in living cells, GFP-tagged ARHGEF10 was expressed in Ig–mCherry-expressing cells, and live-cell images were obtained using confocal microscopy (Fig. 5D; Movie 1). GFP-tagged ARHGEF10 was found to localize to mCherry-positive vesicles and to move toward the cell periphery. These results confirm the localization of ARHGEF10 to Rab6- and Rab8-positive exocytotic vesicles in living cells.

The DH domain, but not GEF activity, is necessary for the localization of ARHGEF10 to exocytotic vesicles

ARHGEF10 acts as a GEF for the RhoA subfamily, as described above (Mohl et al., 2006; Chaya et al., 2011). To examine whether the GEF activity of ARHGEF10 was required for its localization to exocytotic vesicles, we expressed GFP-tagged ARHGEF10 DH-domain mutants in Ig–mCherry-expressing cells. T332I and T332I/L547A are ARHGEF10 mutants with enhanced and suppressed GEF activity, respectively (Chaya et al., 2011). Similar to wild-type ARHGEF10, both mutants were found to localize to Ig–mCherry-positive vesicles (Fig. 5E). By contrast, a DH-domain-truncated mutant (T332I/ΔDH) could not localize to Ig–mCherry-positive vesicles and, instead, was diffusely distributed throughout the cytoplasm (Fig. 5E). These results suggest that the DH domain, but not GEF activity, is necessary for ARHGEF10 localization to exocytotic vesicles.

Journal of Cell Science (2016) 129, 3620-3634 doi:10.1242/jcs.186817

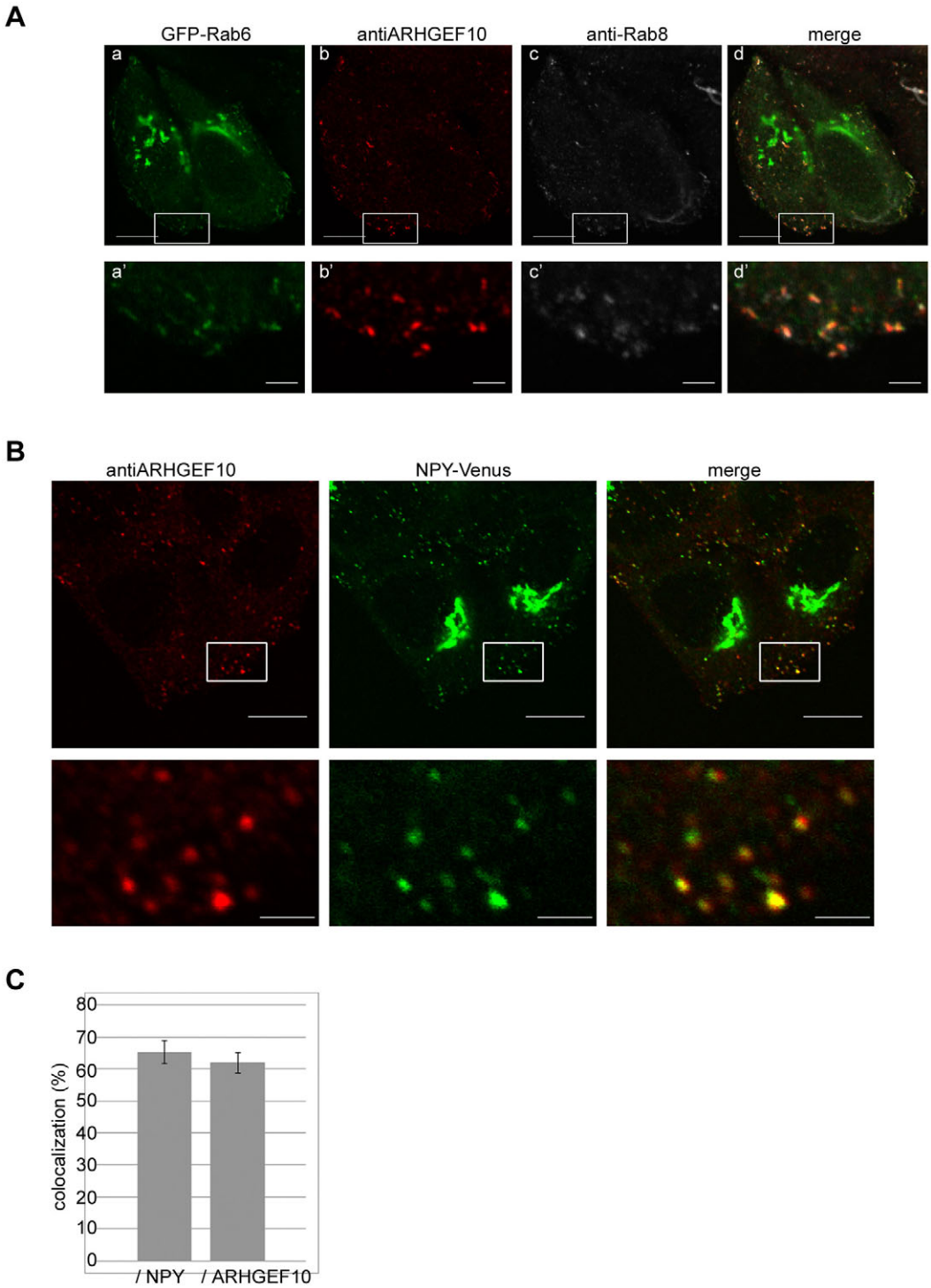

Fig. 4. ARHGEF10 localizes to the Rab6- and Rab8-positive exocytotic vesicles. (A) HeLa cells stably expressing GFP-tagged Rab6a (a and a′) were immunostained with antiARHGEF10 (b and b′) for Rab8 (anti-Rab8, c and c′). Merged images are shown in the right-hand panels (d and d′). A single focal plane was acquired on a confocal microscope. Scale bars: 2 µm. Higher magnification views of the boxed areas are shown in the lower panels (a′–d′). (B) HeLa cells stably expressing NPY–Venus (middle panel, green) were immunostained with antiARHGEF10 (left panel, red). Scale bars: 10 µm. Higher magnification views of the boxed areas are shown in the lower panels. Scale bars: 5 µm. A single focal plane was acquired on a confocal microscope. (C) The percentage of ARHGEF10 localizing vesicles to the total number of NPY–Venus-positive vesicles (left bar, NPY) or the percentage of NPY–Venus localizing vesicles to the total number of ARHGEF10-positive vesicles (right bar, ARHGEF10) was calculated. More than ten cells were examined per assay. Error bars indicate s.e.m.

ARHGEF10 localization is controlled by Rab6a activity

According to a previous study, in which Rab6 depletion appears to disable the localization of Rab8 to exocytotic vesicles, Rab8a localizes to exocytotic vesicles in a Rab6-dependent manner (Grigoriev et al., 2011). To examine whether Rab6 also regulates the localization of ARHGEF10 to exocytotic vesicles, Rab6 was depleted in NPY–Venus-expressing cells, and ARHGEF10 localization in these cells was evaluated (Fig. 6A,B). Notably, the

Journal of Cell Science (2016) 129, 3620-3634 doi:10.1242/jcs.186817

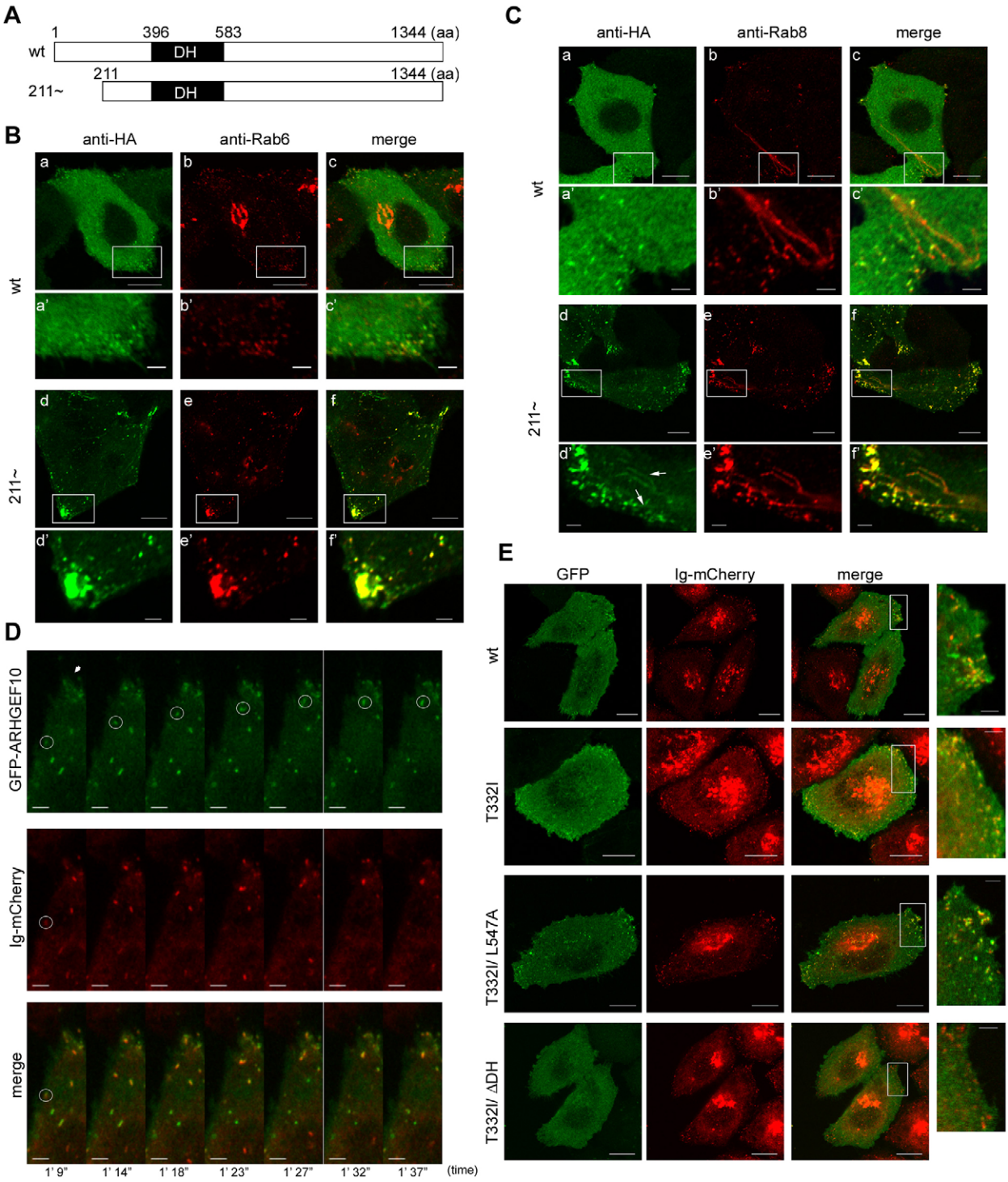

Fig. 5. Localization analysis of exogenously expressed ARHGEF10. (A) Domain structures of ARHGEF10 constructs are depicted. Full-length ARHGEF10 (wt) and a truncation mutant lacking the N-terminal 210 amino acids of ARHGEF10 (211~) are shown. (B) HeLa cells transiently expressing HA-tagged wt (a–c and a′–c′) or 211~ (d–f and d′–f′) were immunostained for HA (anti-HA, a,a′,d and d′) and Rab6 (anti-Rab6, b,b′,e and e′). Scale bars: 10 µm. Higher magnification views of the boxed areas are shown in the lower panels (a′–f′). Scale bars: 2 µm. A single focal plane was acquired on a confocal microscope. (C) HeLa cells transiently expressing HA-tagged wt (a–c and a′–c′) or 211~ (d–f and d′–f′) were immunostained with for HA (anti-HA, a,a′,d and d′) and Rab8 (anti-Rab8, b,b′,e and e′). Scale bars: 10 µm. Higher magnification views of the boxed areas are shown in the lower panels (a′–f′). Scale bars: 2 µm. A single focal plane was acquired on a confocal microscope. Arrows point to tubular structures positive for 211~ and Rab8. (D) HeLa cells stably expressing Ig–mCherry (middle row) were transiently transfected with GFP-tagged ARHGEF10 (upper panels). Merged images are shown in the bottom row. A vesicle, in which both GFP and mCherry signal was found, moving toward the cell edge is indicated by the white circles. The cell edge is indicated by an arrow. Time- lapse images of these cells were taken every 2.28 s for 228 s using confocal microscopy. Scale bars: 5 µm. (E) GFP-tagged full-length ARHGEF10 (wt) or the mutants T332I, T332I/L547A or T332I/ΔDH (left panels) were transiently expressed in HeLa cells stably expressing Ig–mCherry (middle panels). Scale bars: 10 µm. Higher magnification views of the boxed areas are shown in the far-right panels. Scale bars: 2 µm. Images of a single focal plane of GFP and mCherry were obtained using confocal microscopy.

Journal of Cell Science (2016) 129, 3620-3634 doi:10.1242/jcs.186817

number of ARHGEF10-positive vesicles was decreased in Rab6a-depleted cells, with no effect on the number of NPY–Venus-containing vesicles (Fig. 6C,D). Similar results were obtained with the overexpression of a dominant-negative form of Rab6a (Fig. S3C,D). Furthermore, immunoblotting analysis indicated a decrease in ARHGEF10 expression in Rab6-depleted cells. This suggests that ARHGEF10 is unstable in the absence of Rab6. Taken together, these results suggest that Rab6 activity controls ARHGEF10 localization.

ARHGEF10 depletion impairs Rab8 localization to NPY-positive vesicles without affecting Rab6 localization

To confirm the function of ARHGEF10 in Rab6 and Rab8 localization, we knocked down ARHGEF10 and measured the colocalization efficiency between the NPY–Venus signal and endogenous Rab6 or Rab8 in cells that stably expressed NPY–Venus (Fig. 7A,B). ARHGEF10 depletion was confirmed by western blotting (Fig. 7C). ARHGEF10 depletion had no effect on the localization of Rab6 to NPY–Venus-positive vesicles nor on the number of NPY–Venus-positive vesicles (Fig. 7A,D,F). By contrast, knockdown of ARHGEF10 led to a partial decrease in the efficiency of Rab8 colocalization to NPY–Venus-positive vesicles, without affecting the expression of Rab8 (Fig. 7B,C,E). This decrease was rescued by the expression of an RNAi-resistant Myc-tagged mouse ARHGEF10 construct but not by GST–Myc (Fig. 7G–I). These results suggest that ARHGEF10 regulates the loading of Rab8 onto exocytotic vesicles.

To examine whether the GEF activity of ARHGEF10 is related to its ability to localize Rab8 to exocytotic vesicles, Myc-tagged mouse ARHGEF10 mutant L548A, a mouse mutant form corresponding to human to the mutant ARHGEF10 L547A, was expressed in ARHGEF10-depleted cells (Fig. 7G). Expression of Myc-tagged ARHGEF10 was confirmed by western blotting using an antibody against Myc. ARHGEF10 knockdown was verified by western blotting with antiARHGEF10 in Myc-tagged mouse-ARHGEF10-expressing cells. However, this antibody did not detect ectopically expressed Myc-tagged mouse-ARHGEF10. This result indicates that antiARHGEF10 is not able to react with mouse-ARHGEF10 (Fig. 7H; data not shown). Defective Rab8 localization in ARHGEF10-depleted cells was rescued by the mouse L548A mutant to a level comparable to that observed with wild-type ARHGEF10 (Fig. 7I). ARHGEF10 has been reported to act as a GEF for the RhoA subfamily (Mohl et al., 2006; Chaya et al., 2011). In an evaluation to determine whether the expression of a RhoA mutant would affect Rab8 loalization to the exocytotic vesicles, overexpression of RhoA-T19N, a dominant-negative mutant of RhoA, did not alter the localization of Rab8 (Fig. S4A,B). Alternatively, ARHGEF10 might function as a GEF for Rab8 and thus regulate its localization. However, we were unable to detect Rab8 activation during a GEF-activity assay in ARHGEF10-overexpressing cells (Kuroda et al., 2002; Homma and Fukuda, 2016) (Fig. S4C). These results suggest that the GEF activity of ARHGEF10 is not required for its ability to localize Rab8 to exocytotic vesicles.

Depletion of ARHGEF10 induces defects in the ability of cells to invade

It has been previously proposed that, in invading cells, Rab8 resides on vesicles containing MT1-matrix metalloproteinase (MT1-MMP; also known as MMP14), a protease that targets extracellular matrix proteins, mediates the polarized transport of these vesicles from the Golgi to invasive structures and facilitates the focal degradation of extracellular membrane (ECM); in addition, knockdown of Rab8 has been found to inhibit the invasiveness of MDA-MB231 cells (Bravo-Cordero et al., 2007). To investigate whether ARHGEF10 is involved in Rab8-related cell functions, we performed an invasion assay using MDA-MB231 cells in which ARHGEF10 expression and colocalization with both Rab6 and Rab8 were confirmed (Fig. 8A). Similar to Rab8-knockdown cells, ARHGEF10-depleted

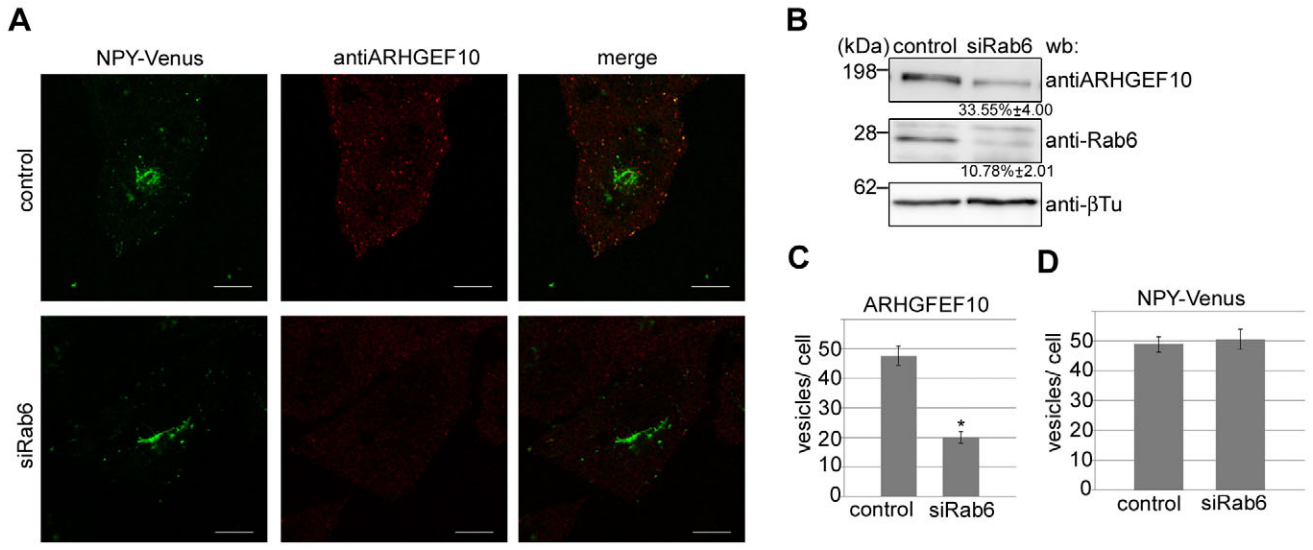

Fig. 6. ARHGEF10 localizes to exocytotic vesicles in a Rab6-dependent manner. (A) HeLa cells stably expressing NPY–Venus (left panels, green) were transfected with control (upper panels) or Rab6a-specific siRNA (siRab6) (lower panels) and immunostained with antiARHGEF10 (middle panels, red). An image of a single focal plane was acquired using confocal microscopy. Scale bars: 10 µm. (B) Expression levels of ARHGEF10, Rab6 and β-tubulin in HeLa cells stably expressing NPY–Venus that had been transfected with control (left lane) or siRab6 (right lane) were analyzed by immunoblotting. Molecular masses in kDa are indicated to the left. Quantified results are shown below each panel. Values are expressed as mean percentages±s.e.m. of the amount of protein from cells that had been treated with control siRNA from three independent experiments. wb, western blot. (C,D) The number of ARHGEF10- (C) or NPY–Venus-positive (D) vesicles per cell was counted using HeLa cells stably expressing NPY–Venus, which had been transfected with control (left) or siRab6 (right). Error bars indicate s.e.m. More than 20 cells were examined per assay. (*P<0.01, Student's t-test.)

Journal of Cell Science (2016) 129, 3620-3634 doi:10.1242/jcs.186817

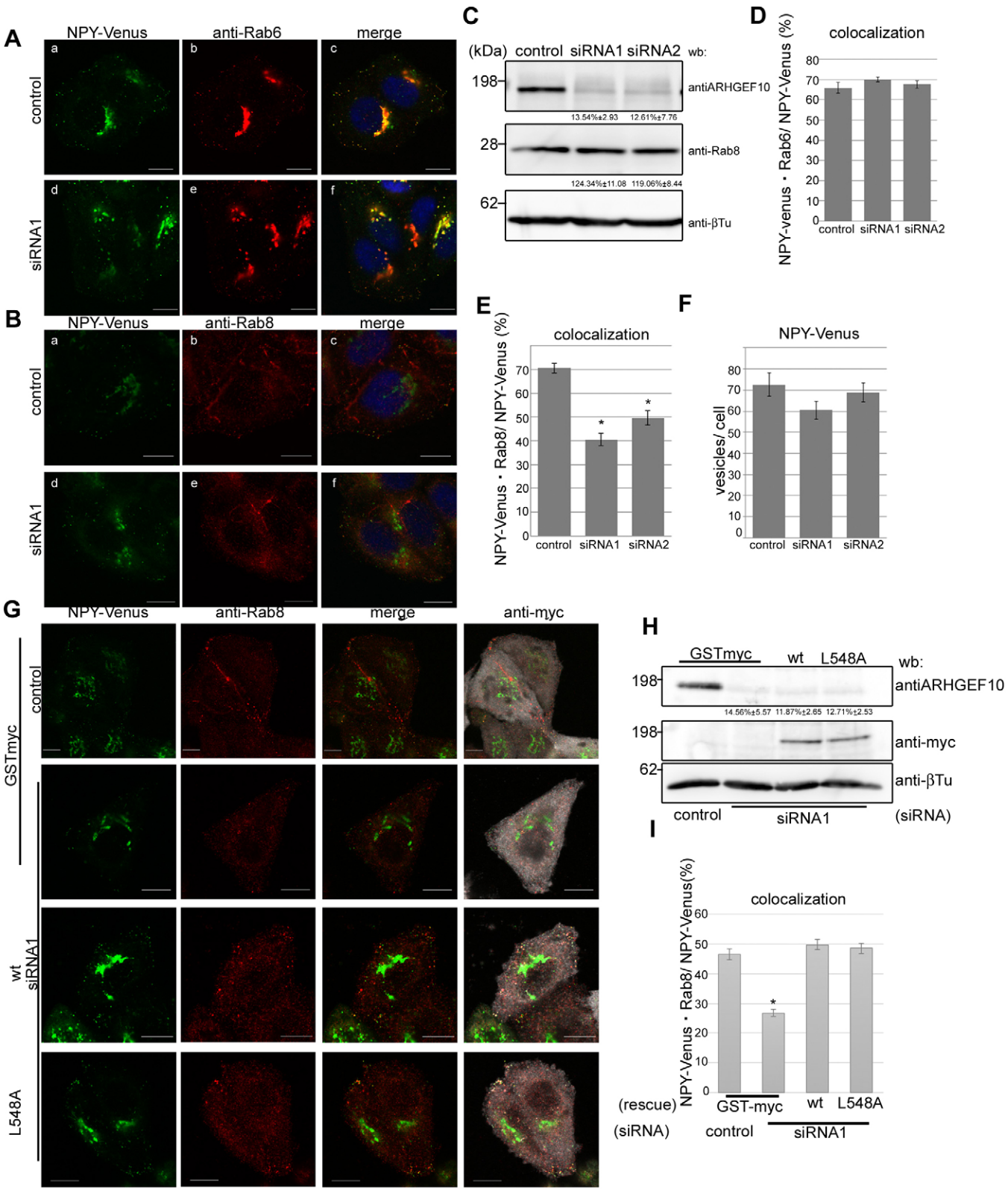

Fig. 7. See next page for legend.

cells exhibited dramatically reduced invasive activity when compared with control cells (Fig. 8B–D). These results suggest that ARHGEF10 might function in the context of cell invasiveness by regulating Rab8 localization.

DISCUSSION

In this study, we demonstrated the localization of ARHGEF10 to Rab6-, Rab8- and NPY–Venus-positive vesicles. These results indicate that ARHGEF10 localizes specifically to Rab6- and Rab8-

Journal of Cell Science (2016) 129, 3620-3634 doi:10.1242/jcs.186817

Fig. 7. Depletion of ARHGEF10 alters the localization of Rab8 but not of Rab6. (A,B) HeLa cells stably expressing NPY–Venus (left panels, green) were transfected with control (upper panels) or siRNA1 (lower panels) and immunostained for Rab6 (anti-Rab6, middle panels, red in A) or for Rab8 (anti-Rab8, middle panels, red in B). An image of a single focal plane was obtained using confocal microscopy. Scale bars: 10 µm. (C) Expression of ARHGEF10, Rab8 and β-tubulin in HeLa cells stably expressing NPY-Venus that had been transfected with control (left lane), siRNA1 (middle lane) or siRNA2 (right lane) was analyzed by immunoblotting. The band intensities were quantified and the ratio of each protein is shown below each panel. Molecular masses in kDa are indicated to the left. Values are expressed as mean percentages±s.e.m. of the amount of protein from cells treated with control siRNA from three independent experiments. (D) The colocalization efficiency of Rab6- and NPY–Venus-positive vesicles in HeLa cells stably expressing NPY–Venus that had been transfected with control, siRNA1 or siRNA2 was calculated. The percentage of both Rab6- and NPY–Venus-positive vesicles of the total number of NPY–Venus-positive vesicles is indicated. Error bars indicate s.e.m. More than 17 cells were examined per assay. (E) The colocalization efficiency of Rab8- and NPY–Venus-positive vesicles in HeLa cells stably expressing NPY–Venus, which had been transfected with control, siRNA1 or siRNA2, was calculated. The percentage of both Rab8- and NPY–Venus-positive vesicles of the total number of NPY–Venus-positive vesicles is indicated. Error bars indicate s.e.m. More than 15 cells were examined per assay (*P<0.01, Student's t-test). (F) The number of NPY–Venus-positive vesicles was counted in the HeLa cells stably expressing NPY–Venus, which had been transfected with control, siRNA1 or siRNA2. Error bars indicate s.e.m. More than 20 cells were examined. (G) HeLa cells stably expressing NPY–Venus (green) were co-transfected with control siRNA and GST–Myc or siRNA1 (directed against ARHGEF10) and GST–Myc, Myc-tagged mouse ARHGEF10 (wild type, wt) or Myc-tagged mouse ARHGEF10 L548A. These cells were immunostained for Rab8 (anti-Rab8, red) and Myc (anti-Myc, gray). Ectopically expressed proteins and transfected siRNA are indicated on the left. Images of a single focal plane were obtained with confocal microscopy. Scale bars: 10 µm. (H) Knockdown of ARHGEF10 and expression of Myc-tagged mouse ARHGEF10 (wild type, wt) and ARHGEF10 L548A were confirmed by immunoblotting with antiARHGEF10 (upper panel), with anti-Myc antibody (middle panel) and anti-β-tubulin antibody (lower panel, anti-βTu). Molecular masses in kDa are indicated to the left. Quantified results are shown below the top panel. Values are expressed as the mean percentage±s.e.m. of the amount of protein from cells treated with control siRNA from three independent experiments. (I) Colocalization efficiency of both Rab8- and NPY–Venus-positive vesicles in the total NPY–Venus-positive vesicle population was calculated. Error bars indicate s.e.m. More than ten cells were examined per assay. (*P<0.01, Student's t-test.)

positive exocytotic vesicles. The finding that the localization of Rab8 to exocytotic vesicles was partially inhibited in ARHGEF10-depleted cells suggests that ARHGEF10 promotes the localization of Rab8 to these vesicles. Furthermore, the invasive activity of MDA-MB231 cells was decreased by depletion of ARHGEF10, as well as of Rab8. These results suggest that ARHGEF10 plays important roles in Rab8-dependent cell functions, such as the tethering and fusion of exocytotic vesicles to the plasma membrane and the establishment of cell polarity, primary cilia and invasive activity (Hattula et al., 2002, 2006; Ang et al., 2003; Bravo-Cordero et al., 2007; Nachury et al., 2007; Sato et al., 2007, 2014; Henry and Sheff, 2008).

Rab8 is known to be involved in not only the tethering and fusion of exocytotic vesicles to the plasma membrane but also in various cellular processes that involve the establishment of cell polarity and primary cilia, which are known to act as sensory organelles, through membrane trafficking events (Hattula et al., 2002; Ang et al., 2003; Nachury et al., 2007; Sato et al., 2007, 2014; Henry and Sheff, 2008). A recent study indicates that Rab8 knockout induces the mislocalization of apical peptidases and transporters to the lysosome in small intestinal cells and leads to the phenotype observed in microvillus inclusion disease (Sato et al., 2007). The relationship of ARHGEF10 with microvillus inclusion disease and intestinal cell polarity in ARHGEF10 KO animals is interesting because Rab8 failed to localize to exocytotic vesicles in ARHGEF10-depleted cells. ARHGEF10 might act in the context of primary cilia formation by mediating Rab8 function. Another previous study has indicated that ARHGEF10 localizes to the centrosome and acts in the regulation of mitotic-spindle formation in HeLa cells (Aoki et al., 2009). In this study, we did not observe the localization of either endogenously or exogenously expressed ARHGEF10 at the centrosome. However, this discrepancy might be attributable to differences in antibodies or cell culture conditions (e.g. serum used in culture medium). Primary cilia project from proximal mother centrioles, which are known as basal bodies (Hsiao et al., 2012). Rab8 localizes to the basal body and plays a crucial role in the formation and function of primary cilia (Nachury et al., 2007; Sato et al., 2014); this suggests that centrosome-localized ARHGEF10 might be involved in primary cilia formation through the modulation of Rab8 function.

In invading cells, Rab8 resides on vesicles containing MT1-MMP, mediates the polarized transport of these vesicles from the Golgi to invasive structures and facilitates the focal degradation of ECM (Bravo-Cordero et al., 2007). The finding that invasiveness was reduced by knockdown of ARHGEF10, as well as of Rab8, suggests that vesicles containing MT1-MMP are aberrantly transported following the failure of Rab8 to localize to the vesicles, which was itself a consequence of ARHGEF10 depletion. Because cell movement in ECM is a very complex process, we could not exclude the possibility that ARHGEF10 functions in non-Rab8-related invasive processes. Various studies have indicated that RhoA activation is necessary for invasive cell migration (Sakurai-Yageta et al., 2008; Friedl and Alexander, 2011; Jacquemet et al., 2013), suggesting that the RhoA GEF activity of ARHGEF10 might be involved in cell invasiveness. Future work will reveal the function of ARHGEF10 in cell invasion.

Previous studies have identified ARHGEF10 as a GEF for the RhoA subfamily (Mohl et al., 2006; Chaya et al., 2011). Does ARHGEF10 act as a GEF in the membrane transport pathway? In this report, an ARHGEF10 mutant (L547A) with decreased RhoA GEF activity (Chaya et al., 2011) was found to localize to NPY-positive vesicles, and overexpression of mutant mouse ARHGEF10 (L548A) restored the localization of Rab8 to NPY-positive vesicles in ARHGEF10-knockdown cells (Figs 5E and 7G). Furthermore, no change in Rab8 localization was observed in HeLa cells that overexpressed a dominant-negative form of RhoA (Fig. S4A,B). Although the residual GEF activity of mouse ARHGEF10 L548A might be sufficient to rescue Rab8 impairment induced by ARHGEF10 knockdown, our results strongly suggest that ARHGEF10 does not behave as a RhoGEF in the membrane transport pathway. Alternatively, ARHGEF10 might be involved in Rab8 activation. However, an assay conducted in ARHGEF10 overexpressing cells failed to detect GEF activity of ARHGEF10 for Rab8 (Fig. S4C). These results suggest that ARHGEF10 might function as a scaffold protein in the membrane transport pathway.

In this report, an immunoprecipitation assay revealed interactions of ARHGEF10 with Rab6 and Rab8 (Fig. 3E). Although ARHGEF10 could apparently interact with all mutant forms of Rab6a, dominant-negative Rab6a exhibited a slightly reduced interaction when compared with constitutively active Rab6a (Fig. S3A,B). These results are consistent with the observation that ARHGEF10 localization is controlled by Rab6a activity (Fig. 6). A pulldown assay involving GST–Rab6 mutants and an ARHGEF10 domain analysis would precisely unravel the mechanisms underlying the interactions of these proteins in the Rab6- and Rab8-related exocytotic pathway.

Journal of Cell Science (2016) 129, 3620-3634 doi:10.1242/jcs.186817

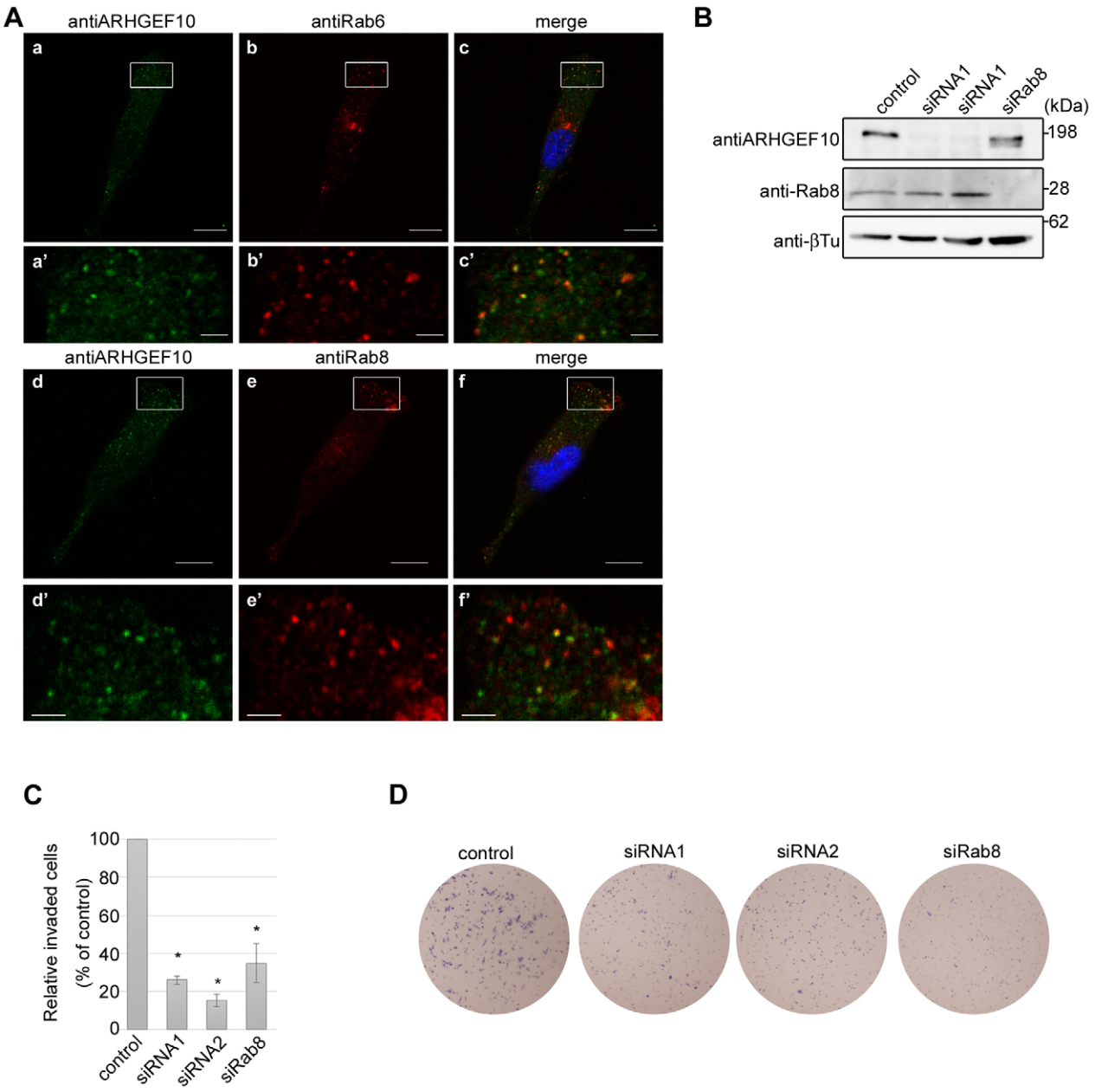

Fig. 8. Knockdown of ARHGEF10, as well as of Rab8, reduces the invasive ability of MDA-MB231 cells. (A) MDA-MB231 cells were immunostained with antiARHGEF10 (a and d) and anti-Rab6 antibody (a–c) or anti-Rab8 antibody (d–f). Scale bars: 10 µm. Higher magnification views of the boxed areas are shown in the lower panels (a′–c′ and d′–f′). Scale bars: 2 µm. Images of a single focal plane were acquired on a confocal microscope. (B) Knockdown of ARHGEF10 or Rab8 were confirmed by immunoblotting with antiARHGEF10 (upper panel), anti-Rab8 antibody (middle panel) and anti-β-tubulin antibody (anti-βTu, lower panel). Molecular masses in kDa are indicated to the right. (C,D) MDA-MB231 cells that had been transfected with control, siRNA1, siRNA2 or Rab8a-specific siRNA (siRab8) were counted and subjected to a Transwell invasion assay using Matrigel. siRNA1 and siRNA2 are directed against directed against ARHGEF10. Cells that had invaded toward the lower side of the Transwell insert after 22 h were stained by Giemsa stain solution, and the number of invaded cells was counted. Values are expressed as mean percentage±s.e.m. relative to those of cells that had been treated with control siRNA from three independent experiments. (*P<0.01, Student's t-test.)

Full-length ARHGEF10 was found to localize to Rab6- and/or Rab8-positive vesicles, whereas an N-terminal-deleted mutant of ARHGEF10 (211∼) additionally resided on Rab8-positive tubular structures (Fig. 5). These results indicate that the N-terminal region of ARHGEF10 inhibits the localization of ARHGEF10 to Rab8-positive tubular structures; in other words, full-length ARHGEF10 might localize temporally and spatially to this tubular structure through certain modifications or interactions with unknown factors in response to a transient stimulation. Indeed, a few ARHGEF10-positive vesicles were observed at or near Rab8-positive tubular structures (Figs 3D and 5C). Furthermore, overexpression of mutant 211∼ induced the appearance of large vesicle-like structures containing both Rab6 and Rab8. How are these large vesicle-like structures generated? Some of these large vesicle-like structures appeared to interact with Rab8-positive tubular structures at the cell periphery (Fig. 5C). Furthermore, these large vesicle-like structures also contained Rab6 and cargo proteins such as NPY–Venus (Fig. 5B; data not shown). Previously,

Journal of Cell Science (2016) 129, 3620-3634 doi:10.1242/jcs.186817

Grigoriev et al. (2011) have reported that once a vesicle exits the Golgi, no exchange of Rab6 occurs until the vesicle has fused with the target site. Accordingly, these large vesicle-like structures might have resulted from fusions between mutant-211∼-positive tubular structures and Rab6-positive vesicles. A more detailed study of these structures would elucidate the molecular mechanism required to generate these large vesicle-like structures and exocytotic vesicles containing both Rab6 and Rab8. Because the localization of Rab8 to secreted vesicles was partially inhibited in ARHGEF10-depleted cells, ARHGEF10 might be involved in the generation of both Rab6- and Rab8-positive vesicles by supplying Rab8 from Rab8-positive tubular structures to Rab6-positive vesicles.

A previous study has found that Rab6- or NPY–Venus-positive vesicles accumulate at the cell periphery in Rab8-depleted cells as a result of inhibited fusion with the plasma membrane (Grigoriev et al., 2011). In our research, we obtained similar results with Rab8-depleted or dominant-negative-Rab8-expressing cells (data not shown). However, we did not observe the accumulation of NPY–Venus-positive vesicles in ARHGEF10-depleted cells, despite the decrease in Rab8-positive exocytotic vesicles (Fig. 7A,B,F). These results suggest that the accumulation of Rab6- or NPY–Venus-positive vesicles observed in Rab8-depleted cells resulted from the depletion of Rab8, which did not localize to exocytotic vesicles (e.g. Rab8 that is diffusely distributed in the cell periphery or localized to the plasma membrane).

Rab8 localization to exocytotic vesicles was partially inhibited in ARHGEF10-depleted cells (Fig. 7). This incomplete inhibition might be attributed to remnant ARHGEF10 expression. Furthermore, Rab8 might localize to exocytotic vesicles through an ARHGEF10-dependent or -independent pathway. Although we used NPY–Venus and Ig–mCherry as secretion markers in this report, new, selective ARHGEF10-regulated exocytotic transport pathways might be elucidated by analyzing ARHGEF10 together with various secretion markers.

A previous report has identified a relationship of the T332I mutant with reduced nerve conduction velocities and peripheral nerve myelination (Verhoeven et al., 2003). Because myelin comprises a specially organized membrane sheet, membrane trafficking might play an important role in the establishment of this structure. In the peripheral nervous system, an endosomal recycling pathway involved in polarized membrane trafficking has been associated with Schwann cell myelination (Roberts et al., 2010; Stendel et al., 2010). In addition, axonal signaling regulates myelin thickness (Michailov et al., 2004; Newbern and Birchmeier, 2010), and this signaling might affect polarized membrane trafficking in Schwann cells. Polarized membrane trafficking to the axon might be required to achieve this signaling. Thus, in the peripheral nervous system, ARHGEF10 might act to establish myelin sheaths by regulating membrane trafficking. Recently, various studies have proposed associations of ARHGEF10 mutations with various diseases, including Charcot–Marie–Tooth disease, epithelial cancer, schizophrenia and atherothrombotic stroke (Cooke et al., 2008; Tabarés-Seisdedos and Rubenstein, 2009; Matsushita et al., 2010; Williams et al., 2010; Yin et al., 2011; Ekenstedt et al., 2014; Boora et al., 2015). More precise studies of ARHGEF10 might identify therapeutic targets for these diseases.

In conclusion, we propose that ARHGEF10 localizes to Rab6- and Rab8-positive vesicles in a Rab6-dependent manner and functions in the exocytotic trafficking pathway by mediating the localization of Rab8. Furthermore, ARHGEF10 is required for cell invasion.

MATERIALS AND METHODS

Antibodies

A mouse monoclonal antibody against ARHGEF10 (antiARHGEF10) was raised against a GST-fused ARHGEF10 fragment containing amino acids 1–405 of ARHGEF10, according to the mouse iliac lymph node method established by Sado (Sado et al., 2006). Rabbit polyclonal anti-γ-tubulin antibodies (Sigma-Aldrich, cat. no. T3320, 1:1000), rabbit polyclonal anti-α-tubulin antibodies (Abcam, cat. no. ab18251, 1:400), mouse monoclonal anti-β-tubulin antibody (Sigma-Aldrich, cat. no. T7816, 1:40,000 for immunoblotting), rabbit monoclonal anti-Rab6 antibody (Cell Signaling, cat. no. D37C7, 1:200 for immunocytochemistry, 1:1000 for immunoblotting), rabbit monoclonal anti-Rab8 antibody (Cell Signaling, cat. no. D22D8, 1:400 for immunocytochemistry, 1:1000 for immunoblotting), mouse monoclonal anti-HA antibody (InvivoGen, cat. no. ab-hatag, 1:1000) were purchased from commercial sources. Fluorescence-labeled secondary antibodies were from Jackson ImmunoResearch (Cy3 and Cy5, 1:1000), Molecular probes (Alexa-Fluor-488, 1:1000) and KPL (DyLight 549, 1 µg/ml). Horseradish peroxidase (HRP)-labeled secondary antibodies were from Jackson ImmunoResearch. Hoechst 33258 was purchased from Nacalai Tesque (cat. no. 04907-91, 1:10,000).

Constructs

The cDNA of human ARHGEF10 and construction of GFP-tagged full-length ARHGEF10, ARHGEF10 T332I, T332I,L547A or T332I,ΔDH have been described previously (Chaya et al., 2011). To construct HA-tagged full-length ARHGEF10 and N-terminal-deleted mutant (lacking residues 1–210) of ARHGEF10, the relevant sequences were PCR-amplified and subcloned into HA-tagged expression vector pCMV-HA. To construct mCherry-tagged ARHGEF10, PCR-amplified full-length *ARHGEF10* was subcloned into the mCherry-tag expression vector pmCherry-C2. The cDNAs encoding mouse ARHGEF10 were obtained by reverse transcription PCR from mouse kidney and subcloned into pBluescript II KS (+) vector. Using this plasmid as a template, full-length mouse *Arhgef10* was amplified by PCR and subcloned into Myc-tagged expression vector pCMV-Myc, thus generating pCMV-Myc mouse ARHGEF10. Mouse ARHGEF10 L548A was generated by PCR-mediated mutagenesis with pBluescript II KS mouse *Arhgef10*. Fragments encoding mouse ARHGEF10 L548A were amplified by PCR and subcloned into pCMV-Myc vector. pEGFP-C1 Rab5a, Rab6a, Rab7, Rab8a, Rab11a and Rab27a were kindly provided by Mitsunori Fukuda (Tohoku University, Aobayama, Aoba-ku, Sendai, Miyagi, Japan) (Itoh et al., 2006; Tsuboi and Fukuda, 2006; Tamura et al., 2009; Ishida et al., 2012; Kobayashi and Fukuda, 2012). pNPY-Venus-N1 was gift from Atsushi Miyawaki (RIKEN, Hirosawa, Wako City, Saitama, Japan) (Nagai et al., 2002). To generate the Ig–mCherry expression vector, fragments encoding mCherry sequence from pmCherry and the NcoI–SalI fragment of Ig k-chain leader sequence from pDisplay vector (Thermo Fisher scientific, Cat. No V660-20) were ligated into the pEF-myc-cyto vector.

Cell culture, siRNA and transfection

HeLa cells and MDA-MB231 cells were cultured in Dulbecco's modified Eagle's medium (DMEM) containing 10% FBS. Lipofectamine 2000 (Thermo Fisher scientific, cat. no. 11668019) was used for transfection of plasmid or siRNA according to the manufacturer's instructions in HeLa cells. In the case of the invasion assay, transfections of siRNA were performed using Lipofectamine RNAi max (Thermo Fisher Scientific, cat. no. 13778150). For rescue experiments, siRNAs and plasmids were co-transfected using Lipofectamine 2000 according to the manufacturer's instructions. To establish stable cell lines, HeLa cells transfected with expression plasmid were cultured in DMEM containing 10% FBS and 700 µg/ml G418 (Sigma-Aldrich, cat. no. G5013-5G). After 2 weeks, GFP- or mCherry-positive colonies were selected. siRNAs were directed against the following target sites: siRNA1 against ARHGEF10, 5′-GGAAACTA-TCAGAACTTAA-3′; siRNA2 against ARHGEF10, 5′-GCAGAGAAGT-TAAATGAAA-3′; siRab6, 5′-GACATCTTTGATCACCAGA-3′ (Young et al., 2005); siRab8, 5′-GGAAAGCACAAATGAAGGA-3′ (Grigoriev et al., 2011). Non-targeting control siRNA was selected as a random

sequence, 5′-ACACCGAAUAACUUUAACCTT-3′ and 5′-GGUUAAA-GU UAUUCGGUGUTT-3′.

Immunoprecipitation

HEK293T cells were co-transfected with pCMV-myc-ARHGEF10 or pCMV-myc (control) and pEGFP-Rab6a-wt, pEGFP-Rab8a-wt, pEGFP-Rab5a-wt or pEGFP-Rab7-wt (where 'wt' denotes wild type) using 1 mg/ml polyethylenimine for 24 h. These cells were washed with PBS and lysed with ice-cold extraction buffer (25 mM Tris-HCl pH 7.5, 150 mM NaCl, 5 mM MgCl, 2 mM EDTA, 1% Triton X-100, 0.1 mM PMSF). The soluble fraction was obtained by centrifuging cell lysates at 20,124 ***g*** for 10 min. The prepared solution was incubated at 4°C with anti-Myc antibody. After 2 h, protein-A–agarose (Sigma-Aldrich, cat. no. P7786-5ML) was added and incubated at 4°C for 1 h, followed by three washes using ice-cold extraction buffer. Bound proteins were eluted by SDS-Sample buffer and analyzed by immunoblotting.

Immunoblotting

Cells were lysed in SDS sample buffer. These samples were loaded onto SDS-PAGE gels and transferred to PDVF membrane (Immobilon-P Millipore Corp., cat. no. IPVH00010). The membranes were blocked with 3% low-fat milk in Tris-buffered saline with Tween-20 (TBST: 20 mM Tris-HCl pH 7.5, 150 mM NaCl, 0.05% Tween-20) and then incubated with primary antibodies. After three washes with TBST, bound antibodies were detected with HRP-labeled secondary antibodies and the ECL detection kit (Nacalai Tesque, cat. no. 02230-30). Images were acquired using an ImageQuant LAS 4000 instrument (GE Health care). Quantification of the intensity of each band was done using ImageQuant TL software.

Immunofluorescence microscopy

HeLa cells on coverslips were transfected and cultured for 2 days and fixed in 4% PFA in PBS for 15 min. Coverslips were then washed with PBS, treated with 0.5% Triton X-100 in PBS for 5 min, blocked with blocking buffer (15 mg/ml BSA, 50 mM glycine, 0. 1% NaN_3 in PBS), incubated with primary antibodies for 2 h and washed four times with PBS. These were incubated with secondary antibodies for 2 h. Then, cells were washed with PBS four times and mounted on glass slides with 80% glycerol in PBS. Antibodies were diluted with the blocking buffer at the aforementioned concentration. To detect γ-tubulin or α-tubulin, cells were fixed with ice-cold methanol for 5 min. Confocal images were obtained with an FV-1000-D IX81 instrument (Olympus) driven by FV10-ASW software (Olympus) and equipped with PlanApo N 60×1.42 NA oil lens. The images were processed with FV10-ASW 4.2 Viewer software, and the adjustments of contrast settings were applied to the whole image. No image filtering was performed. To obtain the live-cell images, HeLa cells stably expressing Ig–mCherry were seeded in a glass-bottomed culture dish (MatTek, cat. no. P35G-0-14-C) and transiently transfected with plasmids encoding EGFP-tagged ARHGEF10 for 48 h. Time-lapse images of these cells were taken every 2.28 s for 228 s with a FV-1000-D IX81 instrument (Olympus) driven by FV10-ASW software (Olympus) and equipped with PlanApo N 60×1.42 NA oil lense. The images were processed and assembled using ImageJ software.

Colocalization

Counting of vesicles was performed using a single focal plane adjacent to a coverslip. Original images were used for counting (image filtering and adjustment of contrast were not performed). To quantify colocalization using HeLa cells that stably expressed GFP–Rab6a, GFP–Rab8a or GFP–Rab11a, all ARHGEF10-positive vesicles and both ARHGEF10- and GFP-positive vesicles in lamella were manually counted. The percentage of vesicles positive for both ARHGEF10 and GFP of the total number ARHGEF10-positive vesicles was calculated. To quantify colocalization using HeLa cells stably expressing NPY–Venus, all ARHGEF10-positive, Venus-positive and ARHGEF10- and Venus-positive vesicles in lamella were manually counted. 40–120 puncta per cell were analyzed. The percentage of vesicles positive for both ARHGEF10 and Venus of the total number of Venus-positive vesicles or total number of ARHGEF10-positive vesicles was calculated. When we calculated the colocalization efficiency of ARHGEF10- and Rab6- or Rab8-positive vesicles at the endogenous level, all ARHGEF10-positive vesicles and both ARHGEF10- and Rab6- or Rab8-positive vesicles in lamella were counted. The percentage of vesicles positive for both ARHGEF10- and Rab6- or Rab8 of the total number of ARHGEF10-positive vesicles was calculated. We confirmed that similar results could be obtained when these experiments were performed in a blinded manner. The mean and the s.e.m. were calculated from data obtained from each cell. Results are representative of three independent experiments. Student's *t*-tests were performed, taking into account the two-tailed distribution and the two-sample unequal variance of the pooled data.

Transwell invasion assay

The Transwell invasion assay was performed as previously described (Hieda et al., 2015). Briefly, 200 µl of 6×10^5/ml cells, which were transfected with siRNA two days before and set on 24-well plates filled with 500 µl DMEM containing 10% FBS (8.0-µm pore size, Falcon, cat. no. 353097), which had been coated with Matrigel (Corning, Cat. No 356234) and set on 24-well plate added 500 µl of DMEM containing 10% FBS. After 22 h, cells were fixed with 4% PFA and stained with Giemsa-stain solution. The images of trans-migrated cells were obtained with a BX53 instrument (Olympus) equipped with UlanSApo 10×0.40 NA lens. All trans-migrated cells in a field for each experiment were counted. Values are expressed as the mean percentage±s.e.m. of the number of cells that had been treated with control siRNA and migrated from three-independent experiments.

Competing interests

The authors declare no competing or financial interests.

Author contributions

antiARHGEF10 was produced by T.T. Localization analysis of ARHGEF10 and Rab6 and establishment of stably expressing cells were performed by T.K. and A.Y. ARHGEF10 mutants were constructed by T.C. and Y.T. Analysis of the cells expressing ARHGEF10 mutants were performed by C.T. Transwell invasion assays were performed by T.H. Immunoprecipitation assays were performed by M.S. GEF assays for Rab8 and blind tests were performed by A.Y. S.I. planned and supervised the experiments. S.S. wrote manuscript and arranged figures.

Funding

This research received no specific grant from any funding agency in the public, commercial or not-for-profit sectors.

Supplementary information

Supplementary information available online at
http://jcs.biologists.org/lookup/doi/10.1242/jcs.186817.supplemental

References

Ang, A. L., Fölsch, H., Koivisto, U.-M., Pypaert, M. and Mellman, I. (2003). The Rab8 GTPase selectively regulates AP-1B–dependent basolateral transport in polarized Madin-Darby canine kidney cells. *J. Cell Biol.* **163**, 339-350.

Anitei, M. and Hoflack, B. (2012). Bridging membrane and cytoskeleton dynamics in the secretory and endocytic pathways. *Nat. Cell Biol.* **14**, 11-19.

Aoki, T., Ueda, S., Kataoka, T. and Satoh, T. (2009). Regulation of mitotic spindle formation by the RhoA guanine nucleotide exchange factor ARHGEF10. *BMC Cell Biol.* **10**, 56.

Boora, G. K., Kulkarni, A. A., Kanwar, R., Beyerlein, P., Qin, R., Banck, M. S., Ruddy, K. J., Pleticha, J., Lynch, C. A., Behrens, R. J. et al. (2015). Association of the Charcot-Marie-Tooth disease gene ARHGEF10 with paclitaxel induced peripheral neuropathy in NCCTG N08CA (Alliance). *J. Neurol. Sci.* **357**, 35-40.

Bravo-Cordero, J. J., Marrero-Diaz, R., Megías, D., Genís, L., García-Grande, A., García, M. A., Arroyo, A. G. and Montoya, M. C. (2007). MT1-MMP proinvasive activity is regulated by a novel Rab8-dependent exocytic pathway. *EMBO J.* **26**, 1499-1510.

Bucci, C., Thomsen, P., Nicoziani, P., McCarthy, J. and van Deurs, B. (2000). Rab7: a key to lysosome biogenesis. *Mol. Biol. Cell.* **11**, 467-480.

Chaya, T., Shibata, S., Tokuhara, Y., Yamaguchi, W., Matsumoto, H., Kawahara, I., Kogo, M., Ohoka, Y. and Inagaki, S. (2011). Identification of a negative regulatory region for the exchange activity and characterization of T332I mutant of Rho guanine nucleotide exchange factor 10 (ARHGEF10). *J. Biol. Chem.* **286**, 29511-29520.

Chen, Y., Wang, Y., Zhang, J., Deng, Y., Jiang, L., Song, E., Wu, X. S., Hammer, J. A., Xu, T. and Lippincott-Schwartz, J. (2012). Rab10 and myosin-Va mediate

insulin-stimulated GLUT4 storage vesicle translocation in adipocytes. *J. Cell Biol.* **198**, 545-560.

Cooke, S. L., Pole, J. C. M., Chin, S.-F., Ellis, I. O., Caldas, C. and Edwards, P. A. W. (2008). High-resolution array CGH clarifies events occurring on 8p in carcinogenesis. *BMC Cancer.* **8**, 288.

Croisé, P., Estay-Ahumada, C., Gasman, S. and Ory, S. (2014). Rho GTPases, phosphoinositides, and actin: a tripartite framework for efficient vesicular trafficking. *Small GTPases* **5**, e29469-1-e29469-15.

Dugani, C. B. and Klip, A. (2005). Glucose transporter 4: cycling, compartments and controversies. *EMBO Rep.* **6**, 1137-1142.

Ekenstedt, K. J., Becker, D., Minor, K. M., Shelton, G. D., Patterson, E. E., Bley, T., Oevermann, A., Bilzer, T., Leeb, T., Drögemüller, C. et al. (2014). An ARHGEF10 deletion is highly associated with a juvenile-onset inherited polyneuropathy in Leonberger and Saint Bernard dogs. *PLoS Genet.* **10**, e1004635.

Friedl, P. and Alexander, S. (2011). Cancer invasion and the microenvironment: plasticity and reciprocity. *Cell* **147**, 992-1009.

Goud, B., Zahraoui, A., Tavitian, A. and Saraste, J. (1990). Small GTP-binding protein associated with Golgi cisternae. *Nature.* **345**, 553-556.

Grigoriev, I., Splinter, D., Keijzer, N., Wulf, P. S., Demmers, J., Ohtsuka, T., Modesti, M., Maly, I. V., Grosveld, F., Hoogenraad, C. C. et al. (2007). Rab6 regulates transport and targeting of exocytotic carriers. *Dev. Cell.* **13**, 305-314.

Grigoriev, I., Yu, K. L., Martinez-Sanchez, E., Serra-Marques, A., Smal, I., Meijering, E., Demmers, J., Peränen, J., Pasterkamp, R. J., van der Sluijs, P. et al. (2011). Rab6, Rab8, and MICAL3 cooperate in controlling docking and fusion of exocytotic carriers. *Curr. Biol.* **21**, 967-974.

Hales, C. M., Griner, R., Hobdy-Henderson, K. C., Dorn, M. C., Hardy, D., Kumar, R., Navarre, J., Chan, E. K. L., Lapierre, L. A. and Goldenring, J. R. (2001). Identification and characterization of a family of Rab11-interacting proteins. *J. Biol. Chem.* **276**, 39067-39075.

Hattula, K., Furuhjelm, J., Arffman, A. and Peränen, J. (2002). A Rab8-specific GDP/GTP exchange factor is involved in actin remodeling and polarized membrane transport. *Mol. Biol. Cell.* **13**, 3268-3280.

Hattula, K., Furuhjelm, J., Tikkanen, J., Tanhuanpää, K., Laakkonen, P. and Peränen, J. (2006). Characterization of the Rab8-specific membrane traffic route linked to protrusion formation. *J. Cell Sci.* **119**, 4866-4877.

Henry, L. and Sheff, D. R. (2008). Rab8 regulates basolateral secretory, but not recycling, traffic at the recycling endosome. *Mol. Biol. Cell.* **19**, 2059-2068.

Hieda, M., Matsuura, N. and Kimura, H. (2015). Histone modifications associated with cancer cell migration and invasion. *Methods Mol. Biol.* **1238**, 301-317.

Homma, Y. and Fukuda, M. (2016). Rabin8 regulates neurite outgrowth in both a GEF-activity-dependent and -independent manners. *Mol. Biol. Cell* **27**, 2107-2118.

Horiuchi, H., Lippé, R., McBride, H. M., Rubino, M., Woodman, P., Stenmark, H., Rybin, V., Wilm, M., Ashman, K., Mann, M. et al. (1997). A novel Rab5 GDP/GTP exchange factor complexed to Rabaptin-5 links nucleotide exchange to effector recruitment and function. *Cell.* **90**, 1149-1159.

Hsiao, Y.-C., Tuz, K. and Ferland, R. J. (2012). Trafficking in and to the primary cilium. *Cilia* **1**, 4.

Hutagalung, A. H. and Novick, P. J. (2011). Role of Rab GTPases in membrane traffic and cell physiology. *Physiol. Rev.* **91**, 119-149.

Ishida, M., Ohbayashi, N., Maruta, Y., Ebata, Y. and Fukuda, M. (2012). Functional involvement of Rab1A in microtubule-dependent anterograde melanosome transport in melanocytes. *J. Cell Sci.* **125**, 5177-5187.

Ishikura, S. and Klip, A. (2008). Muscle cells engage Rab8A and myosin Vb in insulin-dependent GLUT4 translocation. *Am. J. Physiol. Cell Physiol.* **295**, C1016-C1025.

Itoh, T., Satoh, M., Kanno, E. and Fukuda, M. (2006). Screening for target Rabs of TBC (Tre-2/Bub2/Cdc16) domain-containing proteins based on their Rab-binding activity. *Genes Cells.* **11**, 1023-1037.

Jacquemet, G., Green, D. M., Bridgewater, R. E., von Kriegsheim, A., Humphries, M. J., Norman, J. C. and Caswell, P. T. (2013). RCP-driven α5β1 recycling suppresses Rac and promotes RhoA activity via the RacGAP1-IQGAP1 complex. *J. Cell Biol.* **202**, 917-935.

Kobayashi, H. and Fukuda, M. (2012). Rab35 regulates Arf6 activity through centaurin-β2 (ACAP2) during neurite outgrowth. *J. Cell Sci.* **125**, 2235-2243.

Kuroda, T. S., Fukuda, M., Ariga, H. and Mikoshiba, K. (2002). The Slp homology domain of synaptotagmin-like proteins 1-4 and Slac2 functions as a novel Rab27A binding domain. *J. Biol. Chem.* **277**, 9212-9218.

Matsushita, T., Ashikawa, K., Yonemoto, K., Hirakawa, Y., Hata, J., Amitani, H., Doi, Y., Ninomiya, T., Kitazono, T., Ibayashi, S. et al. (2010). Functional SNP of ARHGEF10 confers risk of atherothrombotic stroke. *Hum. Mol. Genet.* **15**, 1137-1146.

Maxfield, F. R. and McGraw, T. E. (2004). Endocytic recycling. *Nat. Rev. Mole. Cell Biol.* **5**, 121-132.

Michailov, G. V., Sereda, M. W., Brinkmann, B. G., Fischer, T. M., Haug, B., Birchmeier, C., Role, L., Lai, C., Schwab, M. H. and Nave, K.-A. (2004). Axonal neuregulin-1 regulates myelin sheath thickness. *Science.* **304**, 700-703.

Miserey-Lenkei, S., Chalancon, G., Bardin, S., Formstecher, E., Goud, B. and Echard, A. (2010). Rab and actomyosin-dependent fission of transport vesicles at the Golgi complex. *Nat. Cell Biol.* **12**, 645-654.

Mohl, M., Winkler, S., Wieland, T. and Lutz, S. (2006). Gef10–the third member of a Rho-specific guanine nucleotide exchange factor subfamily with unusual protein architecture. *Naunyn-Schmiedeberg's Arch. Pharmacol.* **373**, 333-341.

Nachury, M. V., Loktev, A. V., Zhang, Q., Westlake, C. J., Peränen, J., Merdes, A., Slusarski, D. C., Scheller, R. H., Bazan, J. F., Sheffield, V. C. et al. (2007). A core complex of BBS proteins cooperates with the GTPase Rab8 to promote ciliary membrane biogenesis. *Cell.* **129**, 1201-1213.

Nagai, T., Ibata, K., Park, E. S., Kubota, M., Mikoshiba, K. and Miyawaki, A. (2002). A variant of yellow fluorescent protein with fast and efficient maturation for cell-biological applications. *Nat. Biotechnol.* **20**, 87-90.

Newbern, J. and Birchmeier, C. (2010). Nrg1/ErbB signaling networks in Schwann cell development and myelination. *Semin. Cell Dev. Biol.* **21**, 922-928.

Nobes, C. D. and Hall, A. (1995). Rho, rac, and cdc42 GTPases regulate the assembly of multimolecular focal complexes associated with actin stress fibers, lamellipodia, and filopodia. *Cell.* **81**, 53-62.

Ridley, A. J. and Hall, A. (1992). The small GTP-binding protein rho regulates the assembly of focal adhesions and actin stress fibers in response to growth factors. *Cell.* **70**, 389-399.

Ridley, A. J., Paterson, H. F., Johnston, C. L., Diekmann, D. and Hall, A. (1992). The small GTP-binding protein rac regulates growth factor-induced membrane ruffling. *Cell.* **70**, 401-410.

Roberts, R. C., Peden, A. A., Buss, F., Bright, N. A., Latouche, M., Reilly, M. M., Kendrick-Jones, J. and Luzio, J. P. (2010). Mistargeting of SH3TC2 away from the recycling endosome causes Charcot-Marie-Tooth disease type 4C. *Hum. Mol. Genet.* **19**, 1009-1018.

Sado, Y., Inoue, S., Tomono, Y. and Omori, H. (2006). Lymphocytes from enlarged iliac lymph nodes as fusion partners for the production of monoclonal antibodies after a single tail base immunization attempt. *Acta Histochem. Cytochem.* **39**, 89-94.

Sakurai-Yageta, M., Recchi, C., Le Dez, G., Sibarita, J.-B., Daviet, L., Camonis, J., D'Souza-Schorey, C. and Chavrier, P. (2008). The interaction of IQGAP1 with the exocyst complex is required for tumor cell invasion downstream of Cdc42 and RhoA. *J. Cell Biol.* **181**, 985-998.

Sato, T., Mushiake, S., Kato, Y., Sato, K., Sato, M., Takeda, N., Ozono, K., Miki, K., Kubo, Y., Tsuji, A. et al. (2007). The Rab8 GTPase regulates apical protein localization in intestinal cells. *Nature* **448**, 366-369.

Sato, T., Iwano, T., Kunii, M., Matsuda, S., Mizuguchi, R., Jung, Y., Hagiwara, H., Yoshihara, Y., Yuzaki, M., Harada, R. et al. (2014). Rab8a and Rab8b are essential for several apical transport pathways but insufficient for ciliogenesis. *J. Cell Sci.* **127**, 422-431.

Stehbens, S. J., Paszek, M., Pemble, H., Ettinger, A., Gierke, S. and Wittmann, T. (2014). CLASPs link focal-adhesion-associated microtubule capture to localized exocytosis and adhesion site turnover. *Nat. Cell Biol.* **16**, 561-573.

Stendel, C., Roos, A., Kleine, H., Arnaud, E., Ozçelik, M., Sidiropoulos, P. N. M., Zenker, J., Schüpfer, F., Lehmann, U., Sobota, R. M. et al. (2010). SH3TC2, a protein mutant in Charcot-Marie-Tooth neuropathy, links peripheral nerve myelination to endosomal recycling. *Brain.* **133**, 2462-2474.

Stenmark, H., Vitale, G., Ullrich, O. and Zerial, M. (1995). Rabaptin-5 is a direct effector of the small GTPase Rab5 in endocytic membrane fusion. *Cell.* **83**, 423-432.

Sun, Y., Chiu, T. T., Foley, K. P., Bilan, P. J. and Klip, A. (2014). Myosin Va mediates Rab8A-regulated GLUT4 vesicle exocytosis in insulin-stimulated muscle cells. *Mol. Cell Biol.* **25**, 1159-1170.

Tabarés-Seisdedos, R. and Rubenstein, J. L. R. (2009). Chromosome 8p as a potential hub for developmental neuropsychiatric disorders: implications for schizophrenia, autism and cancer. *Mol. Psychiatry* **14**, 563-589.

Tamura, K., Ohbayashi, N., Maruta, Y., Kanno, E., Itoh, T. and Fukuda, M. (2009). Varp is a novel Rab32/38-binding protein that regulates Tyrp1 trafficking in melanocytes. *Mol. Biol. Cell.* **20**, 2900-2908.

Tsuboi, T. and Fukuda, M. (2006). Rab3A and Rab27A cooperatively regulate the docking step of dense-core vesicle exocytosis in PC12 cells. *J. Cell Sci.* **119**, 2196-2203.

Ullrich, O., Reinsch, S., Urbé, S., Zerial, M. and Parton, R. G. (1996). Rab11 regulates recycling through the pericentriolar recycling endosome. *J. Cell Biol.* **135**, 913-924.

Verhoeven, K., De Jonghe, P., Van de Putte, T., Nelis, E., Zwijsen, A., Verpoorten, N., De Vriendt, E., Jacobs, A., Van Gerwen, V., Francis, A. et al. (2003). Slowed conduction and thin myelination of peripheral nerves associated with mutant rho Guanine-nucleotide exchange factor 10. *Am. J. Hum. Genet.* **73**, 926-932.

Williams, S. V., Platt, F. M., Hurst, C. D., Aveyard, J. S., Taylor, C. F., Pole, J. C., Garcia, M. J. and Knowles, M. A. (2010). High-resolution analysis of genomic alteration on chromosome arm 8p in urothelial carcinoma. *Genes Chromosomes Cancer* **49**, 642-659.

Journal of Cell Science (2016) 129, 3620-3634 doi:10.1242/jcs.186817

Yin, Y.-Y., Zhang, B., Zhou, M.-K., Guo, J., Lei, L., He, X.-H., Xu, Y.-M. and He, L. (2011). The functional SNP rs4376531 in the ARHGEF gene is a risk factor for the atherothrombotic stroke in Han Chinese. *Neurol. India* **59**, 408-412.

Young, J., Stauber, T., del Nery, E., Vernos, I., Pepperkok, R. and Nilsson, T. (2005). Regulation of microtubule-dependent recycling at the trans-Golgi network by Rab6A and Rab6A'. *Mol. Biol. Cell* **16**, 162-177.

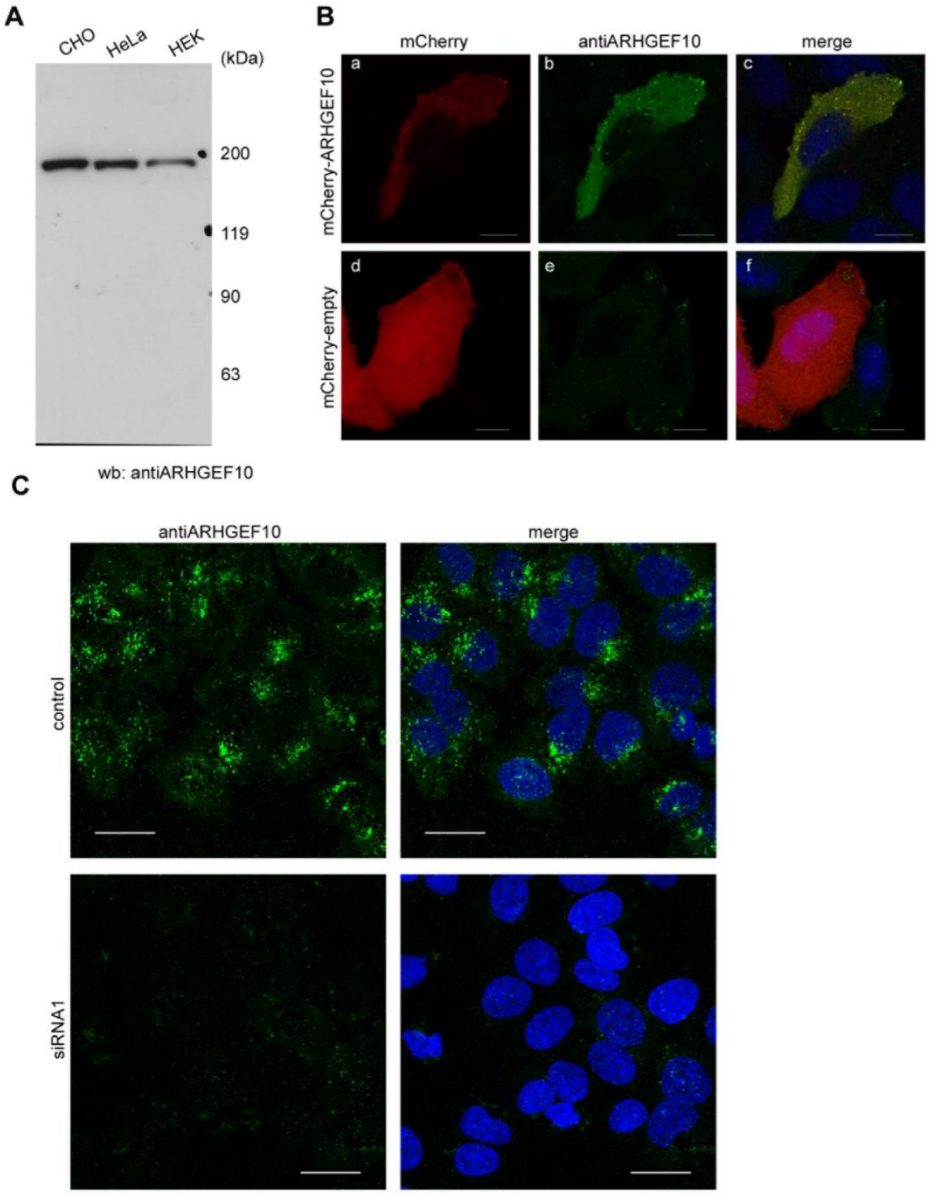

Figure S1. antiARHGEF10 specifically recognized ARHGEF10. A. Protein extract from CHO, HeLa or HEK293T cell were immunoblotted with antiARHGEF10. Bands slightly smaller than 200 kDa were specifically recognized by this antibody. Molecular weights in kDa are indicated to the right. B. HeLa cells transiently expressing mCherry-tagged ARHGEF10 (a) or mCherry (d) were stained with antiARHGEF10 (b and e). Merged images are shown in right panels. A single focal plane images were acquired on a confocal microscopy. Scale bar, 10 μm. C. HeLa cells which had been transfected with control (upper panels) or siRNA1 (lower panels) were treated with nocodazole for 1 hour and fixed by 4 % PFA. Then these cells were immunostained with antiARHGEF10 (right panels) and counterstained by Hoechst 33258. Merged images are shown in right panels. Z-stacked confocal images were acquired on a confocal microscopy. Scale bar, 20 μm.

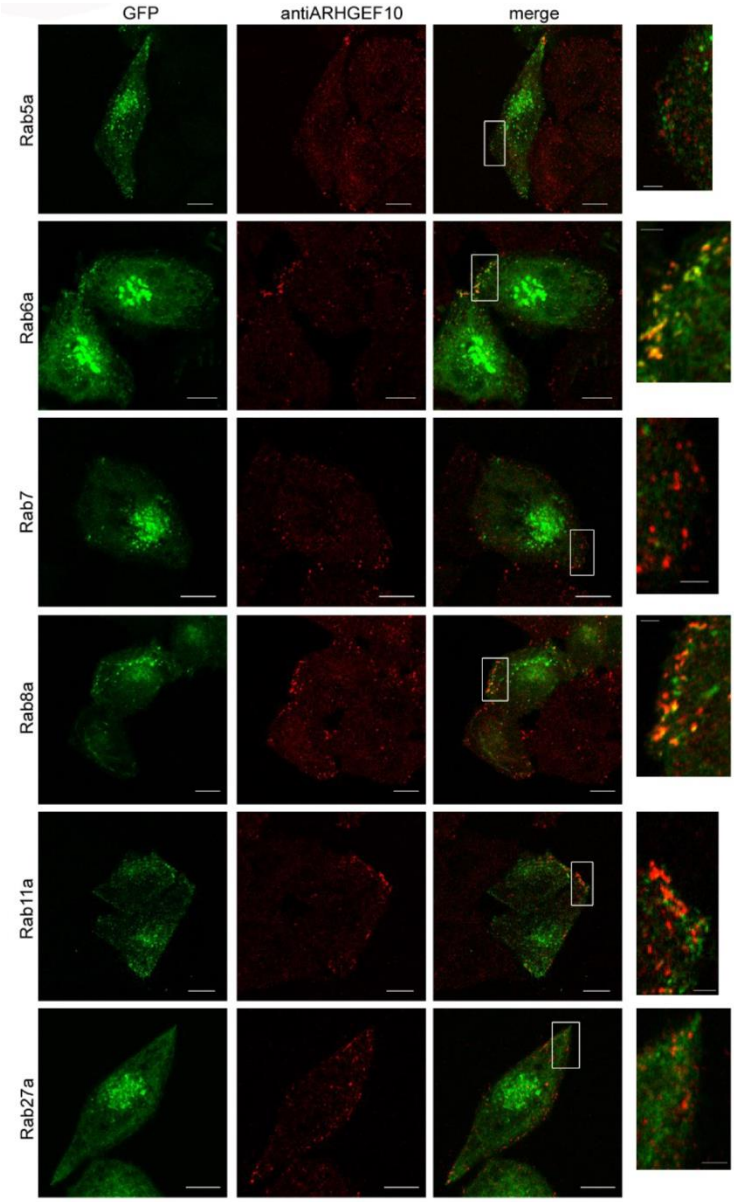

Figure S2. ARHGEF10 was colocalized with GFP tagged Rab6a- and/ or Rab8a-positive vesicles. HeLa cells transiently expressing GFP-tagged Rab5a, Rab6a, Rab7, Rab8a, Rab11a and Rab27a (left panels, green) were immunostained with antiARHGEF10 (middle panels, red). Scale bar, 10 μm. Higher magnification views of the boxed areas are shown in right panels. Scale bar, 2 μm. A single focal plane images were acquired on a confocal microscopy.

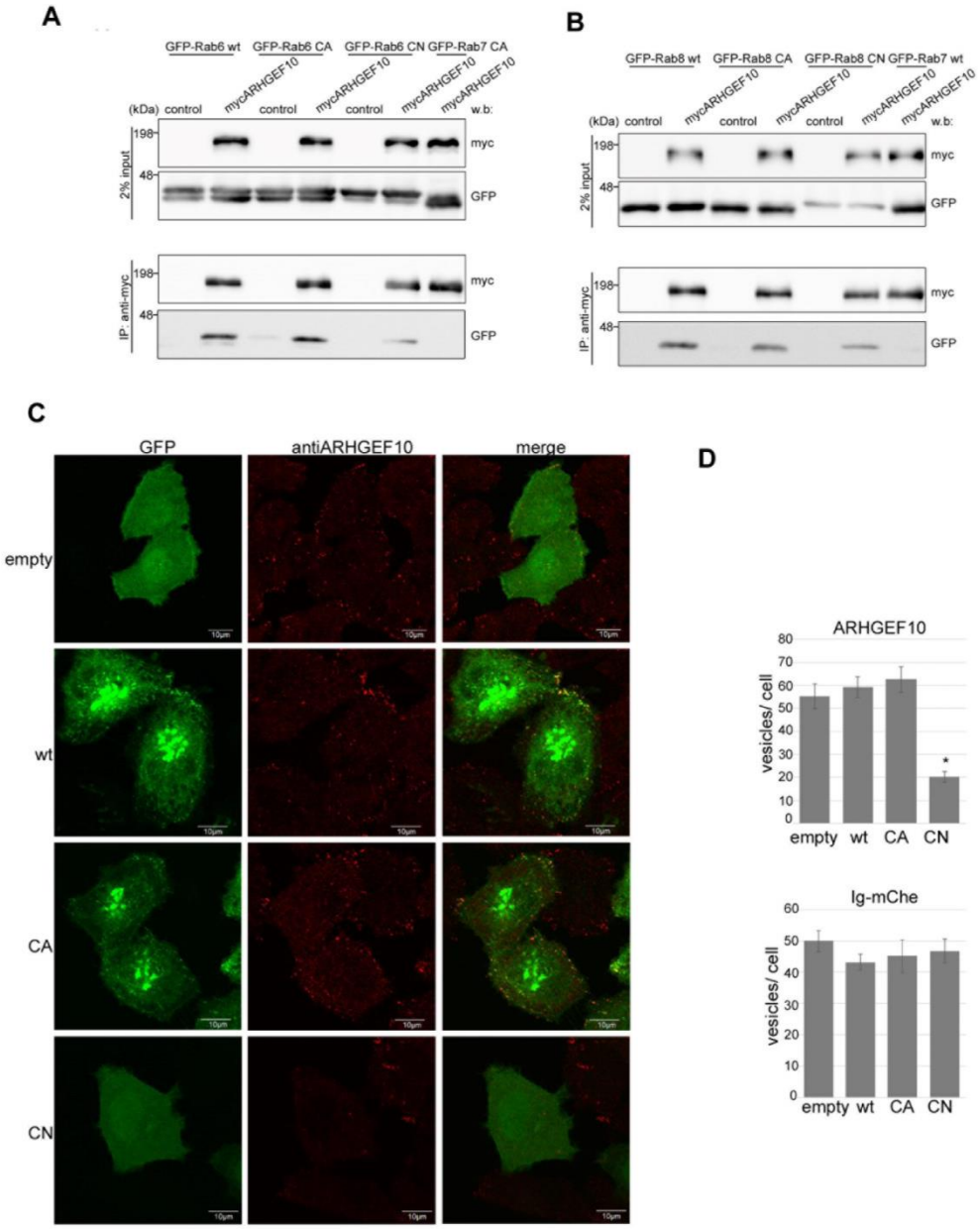

Figure S3. ARHGEF10 interacted with Rab6 and Rab8 and the localization of ARHGEF10 was regulated by activity of Rab6. A. HEK293T cells were co-transfected

with pCMV myc (control) or pCMV myc-ARHGEF10 and EGFP-tagged Rab6a wild type (wt), Rab6a constitutively active form (CA), Rab6a constitutively negative form (CN) or Rab7 constitutively active form (CA) expression plasmids. Total cell lysate (input) were immunoprecipitated by anti-myc antibodies. 2 % total cell lysate and the immunoprecipitates were analyzed by western blotting using anti-myc antibodies and anti-GFP antibodies. Molecular weights in kDa are indicated to the left. B. HEK293T cells were co-transfected with pCMV myc control or pCMV myc-ARHGEF10 and EGFP-tagged Rabs (Rab8a wt, Rab8CA, Rab8CN or Rab7 wt) expression plasmids. Total cell lysate (input) were immunoprecipitated by anti-myc antibodies. 2 % total cell lysate and the immunoprecipitates were analyzed by western blotting using anti-myc antibodies and anti-GFP antibodies. Molecular weights in kDa are indicated to the left. C. HeLa cells transiently transfected with GFP (empty) or GFP tagged Rab6a wild type (wt), constitutively active form (CA) or constitutively negative form (CN) expressing vector (left panels, green) were stained with antiARHGEF10 (middle panels, red). A single focal plane images were acquired on a confocal microscopy. Scale bar, 10 μm. D. The number of ARHGEF10-positive (left) and Ig-mCherry-positive vesicles (right) were counted in these cells. Error bars indicate SE. More than 10 cells were examined per an assay. (*$P < 0.01$ by Student's t-test)

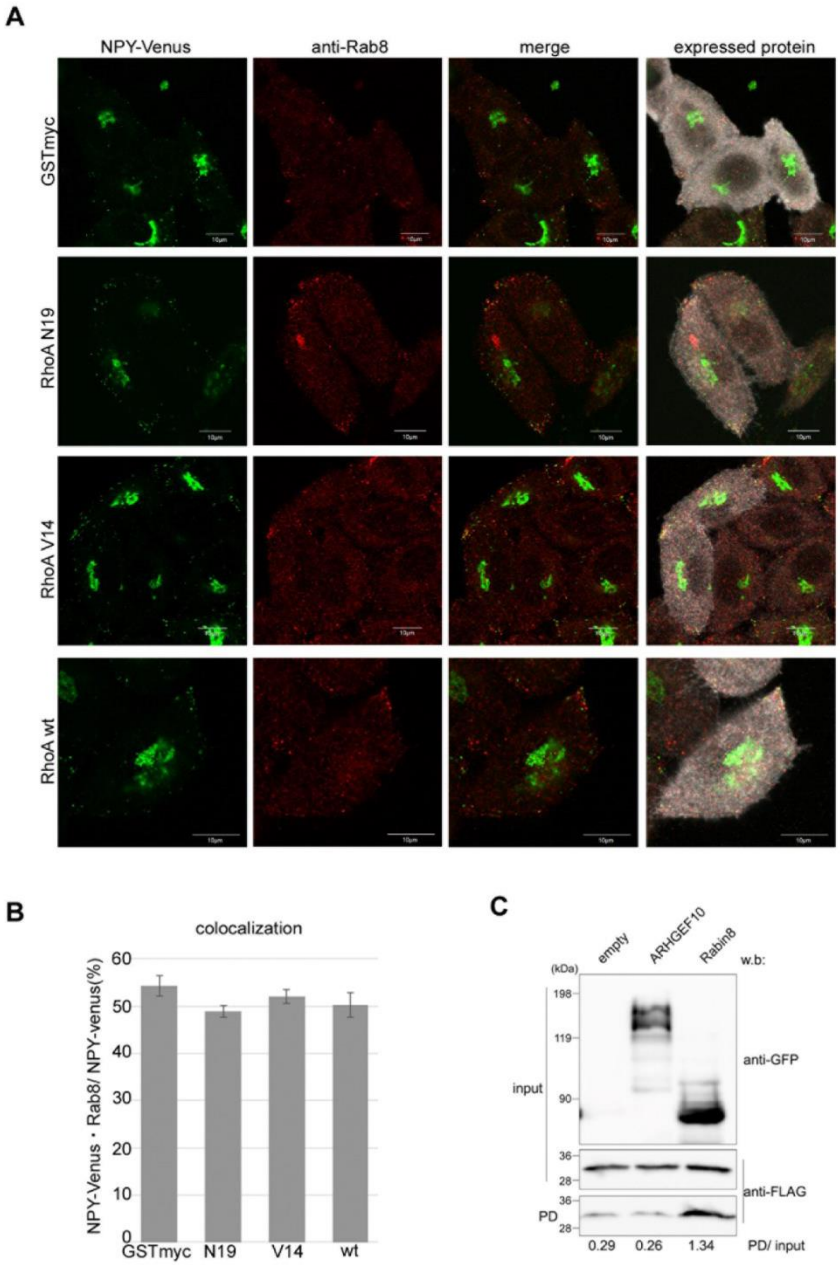

Figure S4. The localization of Rab8 to NPY-Venus-positive vesicle was not influenced by the activity of RhoA and the activation of Rab8 was not found in ARHGEF10 overexpressing cells . A. HeLa cells stably expressing NPY-Venus (green) were transfected with myc-tagged GST (GSTmyc), myc-tagged RhoA dominant negative form (T19N), HA-tagged RhoA dominant active form (G14V) and HA-tagged RhoA wild type (wt) and immunostained with anti-Rab8 antibody (red) and anti-myc antibody (GST and T19N) or anti-HA antibody (G14V and wt) (grey). A single focal plane images were acquired on a confocal microscopy. Scale

bar, 10 μm. B. Colocalization efficiency of Rab8- and NPY-Venus-positive vesicles in HeLa cells stably expressing NPY-Venus, which had been transfected with expression plasmids encoding GSTmyc, RhoA-T19N, RhoA-G14V or RhoA wt, were calculated. Percentage of both Rab8- and NPY-Venus-positive vesicles in total NPY-Venus-positive vesicles were indicated. Error bars indicate SE. More than 17 cells were examined per an assay. C. HEK293T cells were cotransfected with pEF-FLAG-Rab8 and pEGFPC2, pEGFP-C2-ARHGEF10 or pEGFP-C1-Rabin8, which are known as GEF for Rab8. Using these cells, GEF activity assay were performed according to Homma et al.'s method (Kuroda et al., 2002; Homma et al. 2016). In brief, these cells were lysed and active Rab8 was pull-downed by GST-tagged C-terminal fragment of MICAL-L2 (named MICAL-L2 C), which preferentially binds to the active forms of Rab8. The activation of Rab8 were observed in the cells which expressed GFP-Rabin8, but not GFP-ARHGEF10 or GFP. Molecular weights in kDa are indicated to the left. Quantified results are shown below each panel. Values are expressed as PD/ input. Similar results were obtained from three independent experiments.

Movie 1

HeLa cells stably expressing Ig-mCherry (middle panels) were transiently transfected with expression plasmids encoding GFP-tagged ARHGEF10 (left panels). Merged images are shown in right panels. Boxed area indicate the image used in Figure 5D. These images were obtained using confocal microscopy. Time lapse images of these cells were taken at maximum speed. Scale bar, 5 μm.

References

Homma Y. and Fukuda, M. (2016). Rabin8 regulates neurite outgrowth in both a GEF-activity-dependent and -independent manner. *Mol. Biol. Cell*, in press

Kuroda, T. S., Fukuda, M., Ariga, H. and Mikoshiba, K. (2002). The Slp homology domain of synaptotagmin-like proteins 1-4 and Slac2 functions as a novel Rab27A binding domain. *J. Biol. Chem.* **277**, 9212-9218